Journal of Hydrology 662 (2025) 134035

Contents lists available at ScienceDirect

Journal of Hydrology

journal homepage: www.elsevier.com/locate/jhydrol

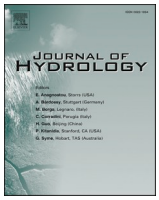

Research papers

A simplified drought indicator based on high-resolution GRACE terrestrial water storage anomalies

Ikechukwu Kalu [a,b,*], Christopher E. Ndehedehe [a,b], Vagner G. Ferreira [c], Sreekanth Janardhanan [d], Matthew Currell [b,f], Oluwafemi E. Adeyeri [e], Onuwa Okwuashi [g], Mark J. Kennard [a,b]

[a] School of Environment & Science, Griffith University, Nathan, QLD 4111, Australia
[b] Australian Rivers Institute, Griffith University, Nathan, QLD 4111, Australia
[c] School of Earth Sciences and Engineering, Hohai University, Nanjing, China
[d] CSIRO Land and Water, Dutton Park, QLD 4102, Australia
[e] ARC Centre of Excellence for the Weather of the 21st Century, Fenner School of Environment and Society, The Australian National University, Canberra, Australian Capital Territory 2600, Australia
[f] School of Engineering and Built Environment, Griffith University, Nathan QLD 4111, Australia
[g] Department of Surveying and Geoinformatics, University of Delta, Agbor, Nigeria

ARTICLE INFO

This manuscript was handled by Marco Borga, Editor-in-Chief, with the assistance of Di Long, Associate Editor

ABSTRACT

Hydrological drought indices based on meteorological data do not fully reflect impacts on hydrological systems, and the coarse spatial resolution of GRACE data limits its usefulness for local-scale drought assessment. To address this, we developed fine-scale drought indices based on Gravity Recovery and Climate Experiment (GRACE)-derived terrestrial water storage anomalies (TWSA) using a statistical downscaling approach. This was achieved by employing a Random Forest machine learning algorithm to integrate key water budget terms (i.e., precipitation, evapotranspiration, runoff and deep drainage) into the original GRACE grids to achieve a drought index at 5 km spatial resolution. The resulting downscaled GRACE drought index (dGdi) is effective for localized drought predictions, providing a comprehensive picture of hydrological and climatic conditions over major river basins in Australia. Application of this downscaled drought index over the Canning Basin, Western Australia, reveals long-term drought evolutions indicating that the region is at a risk of a permanent shift in ecosystem composition (e.g., dominance of drought-tolerant invasive species), land degradation and aquifer depletion. Overall, we found that global climate indices have weak influences on Australia's drought progression. The Back Propagation Neural Network confirmed these indices contribute to drought occurrence in the Canning ($r = 0.37$) and Central Eromanga ($r = 0.36$) Basins. The dGdi developed in this study supports local-scale drought assessment by capturing changes in key biophysical indicators and effectively highlighting intensifying drought patterns. Given its reliance on widely available water budget variables and its adaptability to diverse hydrological settings, the dGdi can be extended to other regions beyond Australia for enhanced drought monitoring and water resource management.

1. Introduction

Drought is a recurring and global complex natural hazard, defined by Van Loon (2015) as a sustained period of below-normal water availability, and driven by a combination of hydrological and atmospheric processes. Its gradual development over timescales ranging from months to decades leads to severe and multifaceted cascading impacts on the environment, often incurring significant economic costs (Kiem et al., 2016; Askarimarnani et al., 2021). The potential for its increased occurrence and long-term persistence in arid regions including but not limited to Australia is significant and could result in severe environmental challenges, such as declines in the availability of surface and groundwater resources. If these declines are not effectively managed, there could be an increased risk of food and water insecurity, wildfires, and other life-threatening environmental consequences (Ndehedehe et al., 2021).

* Corresponding author at: School of Environment & Science, Griffith University, Nathan, QLD 4111, Australia.
E-mail address: ikechukwu.kalu@griffithuni.edu.au (I. Kalu).

https://doi.org/10.1016/j.jhydrol.2025.134035
Received 28 March 2025; Received in revised form 2 June 2025; Accepted 4 August 2025
Available online 6 August 2025

Remote sensing methods are gradually replacing (and/or complementing) traditional methods of ground-based precipitation and evapotranspiration observations for hydrological drought monitoring. This is because they include more climatic factors in their assessment and offer accurate regional and global drought reports, unlike traditional methods that are limited to near-surface or groundwater zones over small areas. The data from the Gravity Recovery and Climate Experiment (GRACE) satellite and its follow-on mission (GRACE-FO) launched in March 2002 and May 2018, respectively, further improved drought estimation from space (e.g., Thomas et al., 2014). GRACE data enhanced our understanding of terrestrial water storage dynamics (ΔTWS), including groundwater storage changes (ΔGWS). For instance, studies have been able to estimate hydrological drought based on total water storage deficit indices (e.g., Liu et al., 2020) and groundwater indices (e.g., Wang et al., 2020) based on GRACE. The study by Liu et al. (2020) detrended ΔTWS to produce a GRACE drought severity index (DSI) free from non-climatic factors over major river basins in China. Their detrended GRACE DSI captured drought processes better than their non-detrended counterparts and agreed very well with well-known indicators, such as the Palmer Drought Severity Index (PDSI), Standardized Precipitation Index (SPI) and the Standardized Runoff Index (SRI). Thomas et al. (2017) developed a GRACE groundwater drought index (GGDI) and was able to highlight critical drought periods over the California Central Valley and linked these droughts to independent drought indices of Standardized Precipitation Index and the Palmer Drought Severity Index.

The potential of GRACE data for drought studies has also been demonstrated globally. Houborg et al. (2012) highlighted the potential of the GRACE data for drought studies by comparing GRACE-based drought indicators to the U.S. Drought Monitor (a data-informed expert assessment of drought intensity and distribution across the USA). They observed a strong relationship between the two indicators, even under the influence of intensive groundwater abstractions. Over the Australian landscape (Fig. 1), Leblanc et al. (2009) employed the GRACE data to quantify the severity of drought over the Murray Darling Basin (MDB) in southeast Australia during the Millenium Drought and reported an estimated 50 % groundwater loss between 2001 and 2007. Their study showed a significant correlation between in-situ groundwater monitoring data and GRACE data, both confirming the 6-year groundwater decline over the study region. Also, Yang et al. (2014) identified a strong decreasing trend over mainland Australia during the Millennium drought from 1997 to 2009 using a GRACE-based indicator. This was confirmed by a decline in the annual mean Normal Difference Vegetation Index (NDVI), which revealed the sensitivity and dependence of ecosystems (reflected by surface greenness) to water availability. With the development of a high-resolution GRACE drought index, our study attempts to improve early-warning capability, local relevance, and the ability to forecast and diagnose contributions of localized climate variability indices which seemed to be lacking in previously developed GRACE-based drought indicators.

This study aims to present a unique perspective on multi-year drought evaluation by developing a high-resolution GRACE drought index. The multi-index drought monitoring technique developed in this study improves upon existing methods, such as the Australian Combined Drought Indicator developed by Guillory et al. (2023), by integrating high-resolution water budget terms into the original GRACE data through statistical downscaling. These water budget terms are representative of localized hydrological fluxes (i.e., precipitation, evapotranspiration, runoff, and deep drainage) that influence drought events over major basins in Australia. With our approach, we intend to

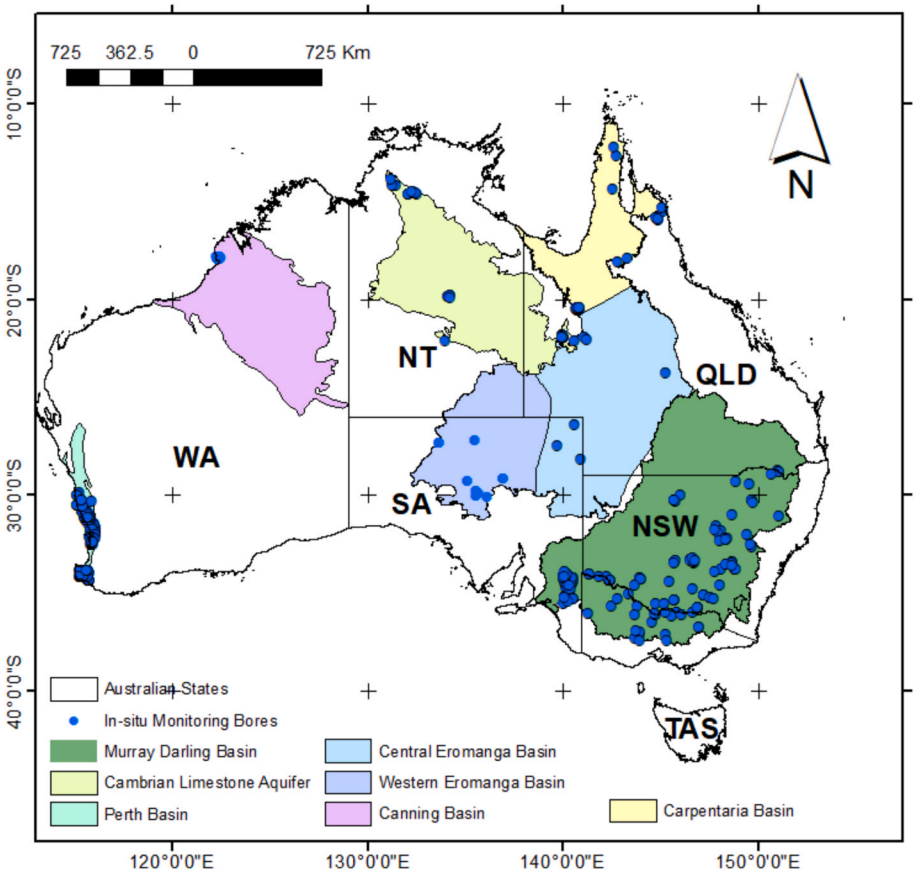

Fig. 1. Study area map showing Australia's major hydrogeological and River Basins and the in-situ monitoring bore locations. These Basins include a large portion of Australia's freshwater reservoirs, including surface and groundwater resources. WA – Western Australia, NT – Northern Territory, SA – South Australia, QLD – Queensland, NSW – New South Wales, TAS – Tasmania.

understand drought evolutions at fine grain sizes of up to 5 km grids. Understanding hydrological drought at such scales is a major knowledge gap and holds the potential to improve the efficiency of hydrological drought estimations. Also, by accommodating more climatic and hydrological drivers of drought progression, this multi-index drought indicator may identify drought patterns over a wider range of hydroclimatic conditions. The specific study objectives included (i) downscaling of monthly GRACE mascon grids to 0.05° using machine learning, (ii) validating the GRACE index in this study with in-situ monitoring bores and well-known drought indicators, including the Standardized Precipitation Evapotranspiration Index (SPEI), Standardized Soil Moisture Index (SSMI), and NDVI, (iii) A deep learning assessment of the contribution and influence of teleconnection patterns from the Indian and Pacific oceans to drought evolutions over the major basins in Australia.

2. Case study

The Australian landscape is highly vulnerable and sensitive to climate change impacts (Peel et al., 2007; Wang et al, 2021). This was recently observed in the duration and intensity of the Australian Millenium Drought, which lasted from the mid-1990 s to 2009, making it the most severe drought event in Australia's history (Van Dijk et al., 2013; Spinoni et al., 2019). This event exacerbated the impacts of the hydrological drought events witnessed from 2006 to 2009 and from 2017 to 2019 (Wang et al, 2021). These frequent drought occurrences highlight the need and urgency to study and evaluate these drought events more critically to guide our expectations about future drought events and increase our chances of drought preparedness and adaptation (Ndehedehe et al., 2021). A detailed summary of the climate, topography, and geology of the studied river basins studied is shown in Table S1.

3. Data

3.1. GRACE terrestrial water storage anomalies

We used the GRACE level 3 mascon (R6v3) product from the Centre for Space Research (CSR), which provides monthly gridded solutions for global terrestrial water storage anomalies. These grids contain water mass anomalies provided as equivalent water thickness from the GRACE time-variable gravity observations for our study period − 2003 to 2022. The equivalent water thickness is an aggregated sum of soil moisture content, surface water (including rivers, lakes, and wetlands), snow content, groundwater and canopy water. Due to GRACE's orbital altitude, the native resolution is obtained at approximately 300 km; however, we used the filtered and processed mascon grid provided by the CSR at a resolution of 0.25° for our analysis. The CSR mascon is based only on GRACE information in the domain of the geodetic grid based on the Tikhonov regularization technique (Save et al., 2016). It undergoes several corrections, including the glacial isostatic and standard corrections for geo-center (degree 1), C20 (degree 20) and C30 (degree 30).

3.2. Water budget terms

The key water budget terms that compose our downscaling framework are fluxes from precipitation, evapotranspiration, runoff and deep drainage. They were obtained from the Australian Water Outlook (AWO) which provides daily gridded model outputs from 1911 to 2024. The AWO integrates diverse climate inputs, advanced downscaling methodologies, post-processing techniques, and the assimilation of near-real-time satellite-derived soil moisture data as inputs to the Australian Water Resource Assessment Landscape (AWRA-L) model (Frost & Shokri, 2021) to produce consistent, high resolution, 5 km hydrological grids across Australia.

The precipitation (PCP) grids were produced from approximately 6,500 rain gauge stations and interpolated to a 0.05° national grid. The estimates are influenced by approximations arising from the interpolation of point-based observational data onto a national-scale grid (Jones et al., 2009). However, they have been reported to meet Australia's water resource needs (Van Dijk, 2010; Frost & Shokri, 2021) and have been adapted as a hybrid modelling framework for hydrological studies (Wilson et al., 2022) across the country.

The evapotranspiration (ET) grids represent the combined water loss through evaporation and plant transpiration, encompassing contributions from vegetation, soil, and groundwater. Water evaporates directly from canopy interception, the upper soil moisture store (depending on the moisture content of the upper soil layer), and the upper surface of the groundwater store (if the water table height exceeds the extinction depth), whereas transpiration withdraws water from the lower soil moisture store, the deep soil store, and shallow aquifers penetrated by vegetation roots. Canopy evaporation follows the event-based model by Gash (1979), incorporating modifications for sparse canopies by Van Dijk and Bruijnzeel (2001).

The runoff (RO) grids represent a modelled estimate of water flow expected from a small, unimpaired catchment area. It is generated from the combined contributions of surface runoff, baseflow, and interflow within each grid cell. As defined by the AWO manual (Frost & Shokri, 2021), surface runoff is a composition of infiltrated and saturated excessive runoff; baseflow depends on groundwater storage and deep drainage from the deep soil storage, while the interflow is the sum of total discharge to the streams from the upper and lower soil stores for each respective grid cell.

Deep drainage (D2) refers to the estimated water flux that percolates from the base of the deep soil layer (below 6 m) into the underlying groundwater stores. The soil drainage and moisture dynamics are modelled based on water balance principles for each soil layer, accounting for the vertical movement of water under gravitational forces in unsaturated conditions. Lateral drainage from the deep soil layer is assumed to be negligible. The available water content and the hydraulic conductivity of the soil constrain the drainage rate for each layer.

3.3. Drought indices

For this study, we used the well-known SPEI and NDVI indices to validate our downscaled GRACE-based drought index (described in section 3.2).

The SPEI is a very useful drought indicator that has the capacity to capture variability in extreme events (very dry and wet conditions) (Ndehedehe et al., 2021). The SPEI data used for our experiment was retrieved from the SPEI database − SPEIbase (*see link in Open Research section*), where global datasets on long-term, high-resolution drought conditions are provided at a spatial resolution of 0.5 degrees and at a monthly time step. For this study, we used the 3-month SPEI estimates, which represent the cumulative effect of rainfall and evapotranspiration over the past three months and are better suited for seasonal drought analysis than other time scales. It was estimated as a standardized variate (mean = 0, variance = 1) based on deviations in the water balance as the difference between actual precipitation and potential precipitation (e.g., Vicente-Serrano et al., 2010). This standardization allows for spatial and temporal comparisons of drought conditions.

The NDVI quantifies the normalized difference in reflectance between the near-infrared (NIR) and visible red spectral bands (Patil et al., 2024). It is widely used in remote sensing as a metric for monitoring vegetation dynamics and assessing vegetation cover on the Earth's surface (Halder et al., 2022). It uses the distinct radiation properties of vegetation, which strongly reflect NIR radiation while absorbing visible red light, to derive a numerical indicator of vegetation health and density.

Since NDVI values are spatially dependent on soil, climate, and topography, ecosystems with more greenness have different radiometric properties compared to those with less greenness. For our study, we

obtained NDVI values from the MOD13A2 V6.1 product (*see link in Open Research section*) at a 1 km resolution. The algorithm for this product selects the best available pixel value from all the acquisitions. The data was provided at a time step of 16 days but was averaged into a monthly time series to be homogenous with the other datasets.

3.4. Root zone soil moisture

Root Zone Soil Moisture reflects the total amount of water stored within the upper and lower soil layers as modelled by the AWRA-L, indicating the proportion of water available in the top 1 m of the soil profile. It estimates the maximum storage within the soil layers from the depth of the soil and the relative soil water storage capacity at high resolution grids of 5 km (0.05°). The soil properties that control this maximum storage are gotten from the continental scale mapping within Australian Soil Resources Information System (Johnston et al., 2003). The relative available water capacity is estimated by dividing the available water content of each soil layer by its thickness.

To estimate hydraulic properties, pedo-transfer functions are applied based on soil texture classifications. Soil water movement and drainage behaviour are modelled using water balance principles applied to each layer. Both shallow- and deep-rooted plant species can access moisture from this aggregated root zone.

3.5. In-situ groundwater bores

In-situ groundwater level (GWL) estimates for each basin were compiled from the Australian Groundwater Explorer database, curated by the Bureau of Meteorology (BOM). The explorer includes ~ 900,000 monitoring bore locations and groundwater levels, providing access to a wide range of groundwater datasets across Australia. For our study, we utilized the 'standing water level (SWL)' variable which measures from the reference point of the bore's top elevation (e.g., the top of the casing) to the water table. Because the SWL values increase positively from the top of the casing to the water table, we performed a scalar multiplication of −1 to all the GWL time series to make them homogeneous to the other datasets. Since the original GWL datasets from the BOM have varying temporal sampling intervals (days to weeks to months), we averaged them into months for the purpose of this study. All data gaps were filled using linear interpolation (Table 1), and the groundwater records were processed and filtered before they were used. Detailed cross validation of the interpolation steps is provided in Table S2. During the processing and filtering, bores less than a year old and bores whose data quality rating flags were below A were removed (BOM, 2015), however, we did not apply this condition to the Canning, Carpentaria, and Western Eromanga Basins. This is because these basins had very limited groundwater records (Table 1), and removal of the data would have otherwise excluded them from consideration in the study.

The data from these bores were used to estimate the groundwater drought severity index and to validate our space-based drought severity index.

Table 1
Properties of the in-situ groundwater monitoring bores used in developing the drought index for our study.

Basin	Number of monitoring bores used	% interpolated
*Canning	15	42 %
*Carpentaria	10	35 %
Central Eromanga	56	11 %
CLA	19	2 %
MDB	254	4 %
Perth	199	2 %
*Western Eromanga	10	20 %

NB: The * shows basins of very high interpolation, which may affect the reliability of their results. interpolation for all basins was done on the original daily datasets before aggregating them to months.

3.6. Climate variability mode

Although the effects of climate conditions on the dynamics of land water storage are seasonal and regionally dependent, they have been identified as a clear contributor to drought events in arid regions such as Australia (Ndehedehe et al., 2021; Devanand et al., 2023). Global climate teleconnections from the Pacific and Indian Ocean likely excerpt strong influences on the Australian continent (Ndehedehe et al., 2023), thus warranting our use of these teleconnection patterns to study their contributions to Australian drought.

The El Nino Southern Oscillation (ENSO) index is obtained from sea level pressure data, sea surface temperature, surface zonal winds, surface meridional winds, and an outgoing longwave radiation dataset over the tropical Pacific basin (30°S to 30°N and 100°E to 70°W) to produce a time series of ENSO conditions for our study duration. The Northern Oscillation Index (NOI) is an index of climate variability on the difference in sea level pressure anomalies in the North Pacific High, a semi-permanent high-pressure system near Darwin, Australia (Schwing et al., 2002). The Oceanic Nino Index (ONI) is one measure of the ENSO, which is simulated from three-month running mean anomalies of Nino 3.4 region (5°N to 5°S and 120°W to 170°W), based on a changing base period consisting of multiple centred 30-year base periods. The Pacific Decadal Oscillation (PDO) is a long-term climate variability pattern in the North Pacific, marked by alternating warm and cool phases of sea surface temperature anomalies over 20 to 30 years. The Quasi-Biennial Oscillation (QBO) is a periodic oscillation of equatorial zonal winds in the stratosphere, calculated using the 30 mb zonal wind averaged at the equator. The Indian Ocean Dipole (IOD) affects the Indian Ocean. During the positive phase, warm waters are propelled to the Western part of the Indian Ocean, while cold, deep waters come up to the surface of the Eastern Indian Ocean (Pillai & Mohankumar, 2010; Krishnamurthy & Krishnamurthy, 2016). This pattern is usually reversed during the negative phase of the IOD. These datasets were retrieved from the NOAA Physical Sciences Laboratory, and the links are provided in the *open research section* of this manuscript.

4. Methods

4.1. Downscaling of GRACE data using machine learning

The CSR Mascon data used in this study were represented on a ¼ degree longitude-latitude grid, but they represent the equal area geodesic grid of size 1 × 1 degree at the equator, which is limited for local scale assessments. Hence, the need for downscaling is evident, as various approaches are available to enhance the spatial resolution of GRACE data (e.g., Miro & Famiglietti, 2018; Ning et al., 2014; Vishwakarma et al., 2021). However, due to the complexity and scale of the data, a machine learning-based downscaling process is developed, specifically designed to produce relatively high spatial resolution GRACE datasets.

Our downscaling approach establishes a regression link between the independent predictor datasets (in this case PCP, ET, RO, D2) and the original GRACE data, which makes them the predictors and predictand, respectively. We used the random forest regression (RFR) method for this operation. The RFR method is an ensemble-based machine learning approach that combines predictions from multiple decision trees to produce an averaged result. This method is usually used in handling non-linear datasets and has been useful in downscaling operations (*see* Agarwal et al., 2023; Kalu et al., 2024a). RFR offers several advantages over traditional regression models, including, being less prone to overfitting, improved feature selection through its ability to assess the importance of input variables, and a more robust internal validation framework. Additionally, the model's hyperparameters can be systematically optimized to enhance performance. We used the Bayesian optimization tool to fine tune the key parameters of the model, such as, the (i) number of trees, (ii) maximum splits, (iii) minimum leaf size and

features considered at each split. We partitioned our dataset into five folds and allotted 70 % data for training and 30 % data for testing in each fold.

The following steps were taken to downscale the GRACE data:

Step 1 – We performed a spatial resampling of the independent variables into the coarse resolution of the original GRACE sample. This was achieved by aggregating 5 (i.e., 0.05°) pixels of the PCP, ET, RO, and D2 datasets to form a single 0.25° pixel like the original GRACE resolution. This action was necessary to achieve consistency in the spatial grain size of independent and dependent variables to enable further operations.

Step 2 – We used the RFR model to establish a regression link between the dependent variable (i.e., original GRACE data) and the independent variables (i.e., PCP, ET, RO, and D2), which have already been spatially aggregated. After this, the model was used to predict GRACE TWSA at 0.25°.

Step 3 – The predicted TWSA in Step 2 was subtracted from the original TWSA to obtain the model residuals for the RFR learning model at a spatial resolution of 0.25°. Using the ordinary kriging method, the residuals were subsequently interpolated to 0.05°.

Step 4 – Afterwards, GRACE TWSA was predicted at 0.05° based on the regression link formed in Step 1. The predicted GRACE TWSA, which reproduces large-scale patterns, was added to the interpolated residuals to form the downscaled GRACE TWSA. This process is referred to as residual correction. It is important to help account for finer scale variations that the RFR predicted TWSA may not capture, even after improving the representation of local scale features.

This downscaling procedure enabled an accurate representation of local scale hydrological dynamics through the adjustment of unmodeled fine-scale variability. It provided high-resolution estimates fused with dynamics of PCP, ET, RO, and D2 (Fig. 2), which were subsequently used to produce fine-scale drought indices.

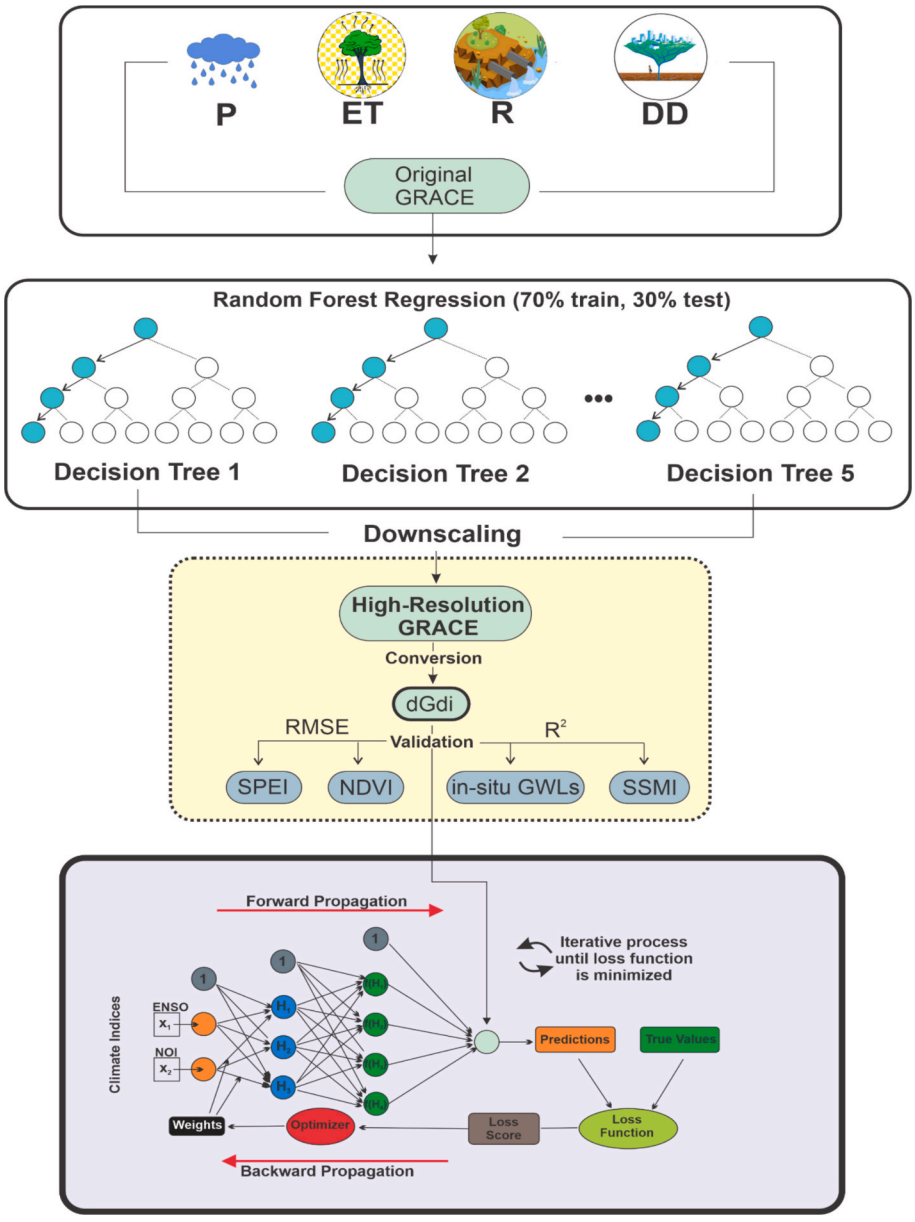

Fig. 2. Flow chart detailing the methods undertaken in our study. The top box represents the predictor and original GRACE datasets used for the downscaling process, the middle boxes depicts the machine learning process for statistical downscaling and the conversion of the downscaled GRACE grids to drought indices (dGdi), the bottom box shows the deep learning process used to identify and predict the impacts of climate variability on the regional hydrology of the sub-basins explored in this study.

4.2. Downscaled GRACE drought index (dGdi)

The drought indicator produced in this study was computed as anomalies of the downscaled GRACE TWSA. It is similar to the TWSA indicator implemented in the Copernicus Global Drought Observatory (GDO), which proved useful for detecting and monitoring long-term hydrological drought conditions (Cammalleri et al., 2019). The dimensionless drought index applied in this study was computed as:

$$dGdi(t) = \frac{DTWS(t) - \overline{X}}{\delta} \quad (1)$$

where, DTWS(t) is the downscaled TWS value for month t, $\overline{X}$ is the long-term averaged TWS values which was from 2004 to 2009, and the δ is the standard deviation. For longer-term drought indicators (e.g., over 100 months), the long-term average is adjusted accordingly with origin for all periods set in January 2003. Prior to operation, the downscaled GRACE TWS values were deseasonalized and detrended using multi-linear regression analysis (see section 3.3). This was to enable the removal of long-term trends due to climate change, land use changes and groundwater depletion. This operation was important to eliminate bias in the estimation of the drought index in this study. After the standardization in eq. (1) was carried out, the drought indices were converted to percentiles by applying the cumulative distribution function (CDF) of the normal distribution, scaled to a range of 0–100 %. This conversion allowed the index to be expressed in percentile terms (Table 2), providing a more consistent representation of anomalies' relative magnitude over time and enabling a detailed interpretation of hydrological variability for each sub-basin. We define the indices based on percentile rank values as per Table 2:

These symmetrical percentile values were based on the drought threshold classification system reported in McKee et al. (1993).

4.3. Regression analysis and teleconnection influence on downscaled GRACE

Due to the strong seasonal variations inherent in GRACE dataset, it was important to deseasonalize and detrend the GRACE data to avoid misinterpretation. To achieve this, we removed the linear trends and harmonic components of the data, which are known to contribute to the seasonal oscillations and trends in GRACE TWS variability (Ndehedehe et al., 2017). We deseasonalized the monthly downscaled GRACE drought index by modelling and removing its dominant cosine and sine harmonic components. This was followed by the method of least squares, which was used to estimate the annual amplitudes of the climate indices (e.g., ENSO, NOI, ONI, PDO, QBO, IOD) on the dGDi. The trend and harmonic component for each basin were removed using multi-linear regression as:

$$Y(i,j,t) = \beta_0 + \beta_1 t + \beta_2 \sin(2\pi t) + \beta_3 \cos(2\pi t) + \beta_4 E(t + \varphi_E) + \varepsilon(t) \quad (2)$$

where, (i,j) represent the spatial grid location, β_0 is the constant offset, β_1 is the linear trend, while β_2 and β_3 account for the harmonic components, β_4 is the amplitude of the downscaled GRACE indices relating to large-scale atmospheric processes and teleconnection patterns, E is the standardized time series of each climate index, and φ_E is the phase lag between each climate index and the downscaled GRACE time series.

Table 2
Downscaled GRACE Drought index categorized based on percentile rank values of index values.

Percentile value	Indices	Category
<2	−2.0 or less	Very Dry
2–20	−1.99 to −0.98	Dry
20–80	−0.99 to +0.99	Normal
80–98	+1.0 to 1.99	Wet
>98	+2.0 and above	Very Wet

$\varepsilon(t)$ represents the random error term.

To estimate the contribution of each of the climate indices on the amplitude of the downscaled GRACE drought values, a least square fit on each grid location was performed (Phillips et al., 2012; Ndehedehe et al., 2017) as.

$$X_{indices}(i,j) = m(i,j) + n(i,j)*indices + c(i,j)*imag(Hilbert(indices)) \quad (3)$$

where, the coefficients, m and n are used to estimate the downscaled drought performance after the impact of climate indices at grid locations i and j, while the unreal part of the Hilbert transform shows the lag between the downscaled drought indices and the climate indices.

4.4. Drought indices for dGdi validation

The dGdi developed in this study was validated using indices from different sources, including in-situ groundwater levels, soil moisture, vegetation (NDVI), and precipitation (SPEI).

4.4.1. In-situ groundwater level indices

The in-situ groundwater level indices generated in this study was based on the analysis of point-scale in-situ groundwater level measurement from the SWL variable across all basins of interest. This index is particularly useful because it helps quantify the impacts of drought resources and can be used to develop early warning systems. It is also important to validate the dGdi which is expected to detect groundwater droughts.

Prior to the index estimation, the in-situ GWL time series underwent deseasonalization to remove regular seasonal fluctuations and detrending to eliminate long-term shifts that obscure short-term anomalies. Following these preprocessing steps, the anomaly values were standardized using Eq. (1), which were subsequently classified into drought categories based on their percentile ranks as shown in Table 2.

4.4.2. Standardized soil moisture indices

The standardized soil moisture indices (SSMI) generated in this study was based on the estimation of the root zone soil moisture (at 0.05° spatial resolution) quantity across all the basins of interest. This SSMI is helpful in drought studies due to its proficiency in assessing soil moisture anomalies by comparing current conditions to long-term climatological norms. For this study, we only considered the upper (top 10 cm) and lower (between 10 cm and 100 cm) layers of the soil profiles because the deep layer (between 1 m and 6 m) were poorly quantified by AWRA-L due to limited availability of quality data to define the soil properties at this depth. This helped to eliminated bias and uncertainty in SSMI as a validation tool. After the deseasonalizing and detrending operations, the values were standardized based on equation on Eq. (1) and categorized based on the percentile rank values shown in Table 2.

4.4.3. Vegetation (NDVI) and precipitation (SPEI)

Given that these are conventional indices that have been widely used in past drought studies (Chen et al., 2014; Shi et al., 2020), we did not apply much pre-processing steps to them, except for the deseasonalizing and detrending of the NDVI. The SPEI was used in its native form.

4.5. BPNN model for climate-hydrology relationship

We used the backpropagation neural network (BPNN) to identify and predict the impacts of climate variability on regional hydrology over the sub-basins explored in this study. The BPNN uses a probabilistic approach for optimization. In relation to the traditional artificial neural network (ANN), it has a flexible topological framework, and explainable learning process, and has been observed to minimize possible overfitting (Kalu et al., 2022). Using its multi-layer perceptron procedure, we linked the ENSO, NOI, ONI, PDO, QBO and IOD indices to the dGdi through a series of successively arranged hidden layers, made up of non-

linear elements called neurons.

For our modelled BPNN, we created a 3-neuron layer framework, with one input layer, 10 sets of hidden layers (2 neurons each), and an output layer (1 neuron). The net input for each discrete neuron in the hidden layer is a total of all the input values, each multiplied by its weight (w) and bias (z) term. This can also be referred to as a unit weight from an auxiliary input (Goethals et al., 2007). The hidden layer network can be summarized as:

$$\begin{aligned} H_1 &= \sum_{i=1}^{n} w_a.X + z_a \rightarrow H_2 = f(H_1) \\ H_2 &= \sum_{i=1}^{n} w_b.X + z_b \rightarrow H_3 = f(H_2) \\ H_3 &= \sum_{i=1}^{n} w_c.X + z_c \rightarrow H_4 = f(H_3) \\ &\vdots \\ H_{10} &= \sum_{i=1}^{n} w_j.X + z_j \rightarrow Y = f(H_{10^*}) \end{aligned} \tag{4}$$

where, the hidden layers are represented as H_1 to H_{10}, with auxiliary variables w_a to w_j and z_a to z_j depicting the varying weights and bias terms for each layer, respectively. The number (n) of neurons for each layer is limited to 2, causing each layer to iterate twice, therefore n = 4. X and Y represent the input (climate teleconnection patterns) and output (downscaled GRACE drought index) neurons for the BPNN. H_{10^*} represents the net input for each discrete neuron in the hidden layer totalling all the input values from the input layer (X) to hidden layer 9. This means that, while $Y = f(H_{10^*})$ is the output which is directly a function of the 10th hidden layer, it is indirectly a function of the entire BPNN model (Kalu et al., 2022). For this experiment, 70 % of the data was randomly selected for training and 30 % was selected for testing across all the study areas (Fig. 2).

4.6. Model performance evaluation and correlation analysis

To evaluate the performance of the downscaled drought index developed in this study, we applied the root means square (RMSE) statistics, which has been widely applied in ascertaining the performance evaluation of several hydrological models (e.g., Kalu et al., 2024b).

$$RMSE = \sqrt{\frac{1}{n}\sum_{i=1}^{n}(dGdi_i - GWL_i)^2} \tag{5}$$

where, n represents the total number of estimates in months, dGdi is the downscaled GRACE drought index, and GWL is the groundwater level for each respective basin. Note that the GWL values here has been converted to indices as in the dGdi for a better comparison.

Using Spearman's rank correlation, we measured the strength and direction of monotonic association between the dGdi and GWL values, SPEI, and NDVI to assess how well they relate to each other.

$$r_s = 1 - \frac{6\sum d_i^2}{n(n^2-1)} \tag{6}$$

where, d_i^2 is the difference between the ranks of the dGdi, SPEI, NDVI, and GWL values, while n is the number of estimates in months.

5. Results and discussion

Verifying the accuracy of downscaled GRACE data is inherently challenging due to its global nature and the complexity of interpreting large-scale hydrological information (e.g., Ferreira et al., 2023). Also, because the GRACE data is unique, with no ground truth dataset available, several approaches have been utilized in previous studies to validate downscaled GRACE data, including the mass conservation approach (Vishwakarma et al., 2021), the water budget approach (Adeyeri et al., 2024; Kalu et al., 2024b), and the use of in-situ precipitation measurements (Kalu et al., 2024a). Each method provides valuable insights but comes with limitations. In our study, however, we focus on validating the dGdi with in-situ groundwater estimates, SSMI and well-known indices of SPEI and NDVI. Given that the dGdi was derived from the original GRACE TWSA, our approach is essential to align our validation strategy with the specific characteristics of this drought indicator.

5.1. Validation of downscaled GRACE drought index using in-situ groundwater monitoring and SSMI

Fig. 3 illustrates the validation process by comparing the dGdi with in-situ groundwater data and SSMI. For best comparisons, a similar index for the groundwater readings were computed and used for this validation. The yellow vertical line in the figure marks the heavy rainfall event in southeast Australia, which contributed to the end of the Millennium Drought era. This event was significant not only for its regional impact but also for the contrast it provided with rainfall patterns in the Northern Territory, an area that did not experience the millennium drought. By correlating the observed shifts in the GRACE drought index with the timing of this heavy rainfall, we were able to assess the accuracy of the downscaled drought estimates in reflecting real-world hydrological changes. This validation approach, which uses the SSMI and in-situ groundwater measurements against the dGdi, ensures that our downscaled product remains consistent with observed hydrological conditions and at a similar spatial resolution. The results confirm that the downscaled GRACE drought index successfully captured droughts' spatial and temporal dynamics in the basins.

We observed a weak correlation between dGdi and in-situ GWLs during the drought era for most of the basins (Fig. 3). This is caused mainly by the weak surface and soil moisture contributions to GRACE signals during this period, leading to weaker representation of groundwater-only changes by GRACE. Additionally, groundwater systems often respond slowly to drought conditions due to delayed recharge and the influence of the aquifer properties, including storage coefficients and specific yield, which may not align temporally with the broader changes observed by GRACE. Albeit, it is important to note that there is evidence that instantaneous poro-elastic response dominates in confined aquifers, whereas in unconfined aquifers, the lag-time associated with recharge is an important control on level changes (Burgess et al., 2017; Kalu et al., 2024c).

However, these trends shifted after the heavy rains in 2009 and 2010 that provided a more reliable water balance, thus improving the correlation between GRACE and in-situ groundwater bores in Fig. 3. The regions not significantly affected by the Millenium drought maintained an average correlation of r = 0.40 between GRACE and in-situ monitoring bores over the entire study period (i.e., 2003 to 2022). For example, the Canning Basin (Fig. 3a), CLA (Fig. 3d), and the Perth Basin (Fig. 3f). A similar observation was observed between dGdi and SSMI, where correlation values were generally lower before drought episodes and higher after them, as seen in the Canning, Central Eromanga, CLA, MDB, and Perth Basins. However, over the MDB, the correlation between dGdI and SSMI strengthened after the heavy rains, while the correlation between dGdi and in-situ groundwater levels weakened during the same period. This suggests that drought episodes in the MDB after the impacts of the heavy rains of 2010 were dominated by agricultural drought, with limited groundwater depletion, indicating that soil moisture deficits were more prominent than declines in groundwater levels (Fig. S1). This interpretation is plausible, as the dGdi can differentiate between various drought types and tends to respond most to the dominant drought signal at any given time.

The Carpentaria and CLA basins maintained the strongest annual correlation between dGdi and in-situ monitoring stations at r = 0.69 and r = 0.62, respectively. (Fig. 4b – Note that the data quality for this basin is poor until 2010). For the MDB, we observed strong consistency between dGdi and in-situ monitoring stations. It showed a near-drought period between 2003 and 2009, a wet (recharge) period between

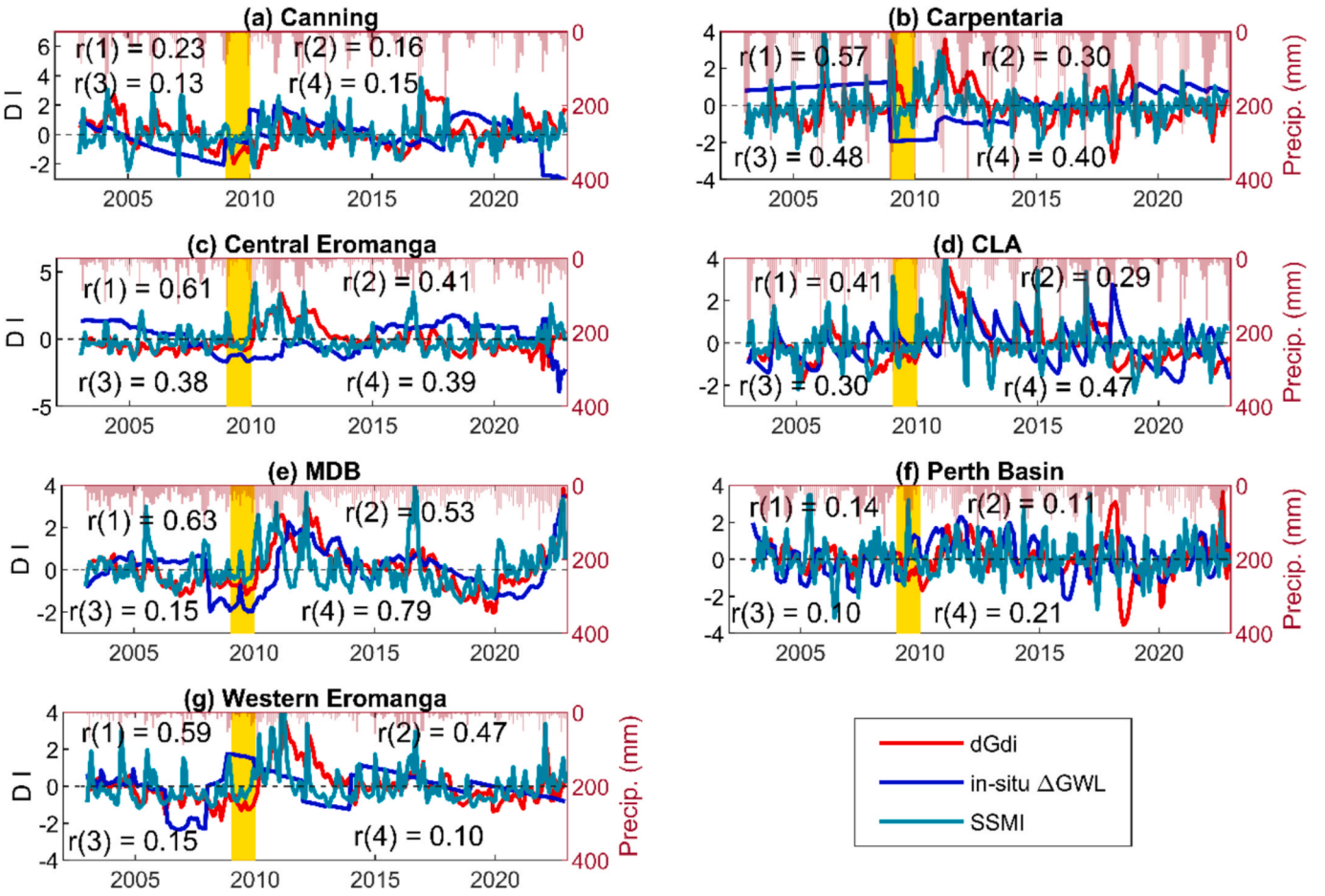

Fig. 3. Monthly comparison of the downscaled GRACE index against in-situ monitoring bores and the standardized soil moisture index (SSMI). These monitoring bores are aggregated/averaged levels for each respective bore. The yellow vertical line highlights the heavy rainfall that was witnessed within southeast Australia, which ended the Millenium drought era. Coincidentally, heavy rainfall was also observed in the Northern territory (Fig. 3d, 3 g) which did not experience the Millenium drought. The dGdi is shown in red, while the in-situ GWL and SSMI are shown in blue and cyan, respectively. The averaged precipitation is shown in dark red bars. r(1) and r(2) represent the correlation between the dGdi and the in-situ GWLs during the drought (2003 to 2009) and the post-drought (2010 to 2022) eras, respectively, while r(3) and r(4) represent the correlation between the dGdi and the SSMI during the drought and post-drought eras, respectively. D. I stands for Drought indices. (For interpretation of the references to colour in this figure legend, the reader is referred to the web version of this article.)

2009 and 2012, and a steady decline to another near-drought period between 2012 and 2019. Beyond 2019, we observe another recovery level in the MDB in response to the Government's effort to protect the Basin from experiencing severe drought, given that it supplies freshwater to over 2.4 million Australian residents. The Perth, CLA, and MDB showed the smallest root mean square error (RMSE) at 0.62 mm, 0.70 mm, and 0.73 mm, respectively. This was mostly due to the availability of in-situ monitoring records which limited interpolation in these basins (Table 1).

Also, we observed much stronger relationships between dGdi and SSMI (compared to in-situ GWLs) across some basins, including the Canning, Central Eromanga, and Western Eromanga. This indicates that these basins experienced agricultural drought episodes (linked to root-zone soil moisture) more frequently than groundwater drought. Overall, we observed that dGdi mostly aligned with SSMI than the in-situ groundwater drought indices for some of the basins (e.g., Canning, Carpentaria, Central Eromanga, CLA and Western Eromanga), suggesting shallow soil moisture stress rather than long-term groundwater depletions in these basins. The corresponding RMSE values support these findings, showing consistently lower errors for SSMI compared to groundwater in most basins, especially where correlation with groundwater is low. The CLA and Carpentaria basins show strong alignment across the SSMI and groundwater indicators likely due to a more responsive or shallow groundwater system.

We also observe the relationship between the annual amplitudes of precipitation patterns and the dGdi. These annual precipitation amplitudes align well with wet and dry signals of the dGdi for most basins, especially those where drought episodes are not driven by excessive groundwater withdrawals. For example, in the Carpentaria Basin (Fig. 4b), a strong annual rainfall was recorded between 2009 and 2011, resulting in a positive dGdi during this period (i.e., nearing very wet conditions). The same was observed in Central Eromanga (Fig. 4c), CLA (Fig. 4d), MDB (Fig. 4e), Perth Basin (Fig. 4f), and the Western Eromanga Basins (Fig. 4g). The strong rainfall during the 2009 and 2011 period propelled the dGdi of these basins into wet and very wet conditions. For the Canning Basin (Fig. 4a), however, a spike during this period was observed, but the dGdi did not go beyond the normal condition, but in 2017, the dGdi spiked into a very wet condition. This spike might be due to human influences as rainfall remained normal in the basin and other nearby basins during this spike period. The Canning and Western Eromanga Basins have the lowest annual rainfall rates in our study region, making them highly vulnerable and susceptible to prolonged drought episodes in the long term. On the other hand, the Carpentaria receives the most rainfall and has shown very normal conditions throughout the study period. However, climate change impacts and over-reliance on the basin's ground and surface water resources for agriculture, mining, and industries could potentially increase the risk of reduced water availability in the future. Overall, most of the

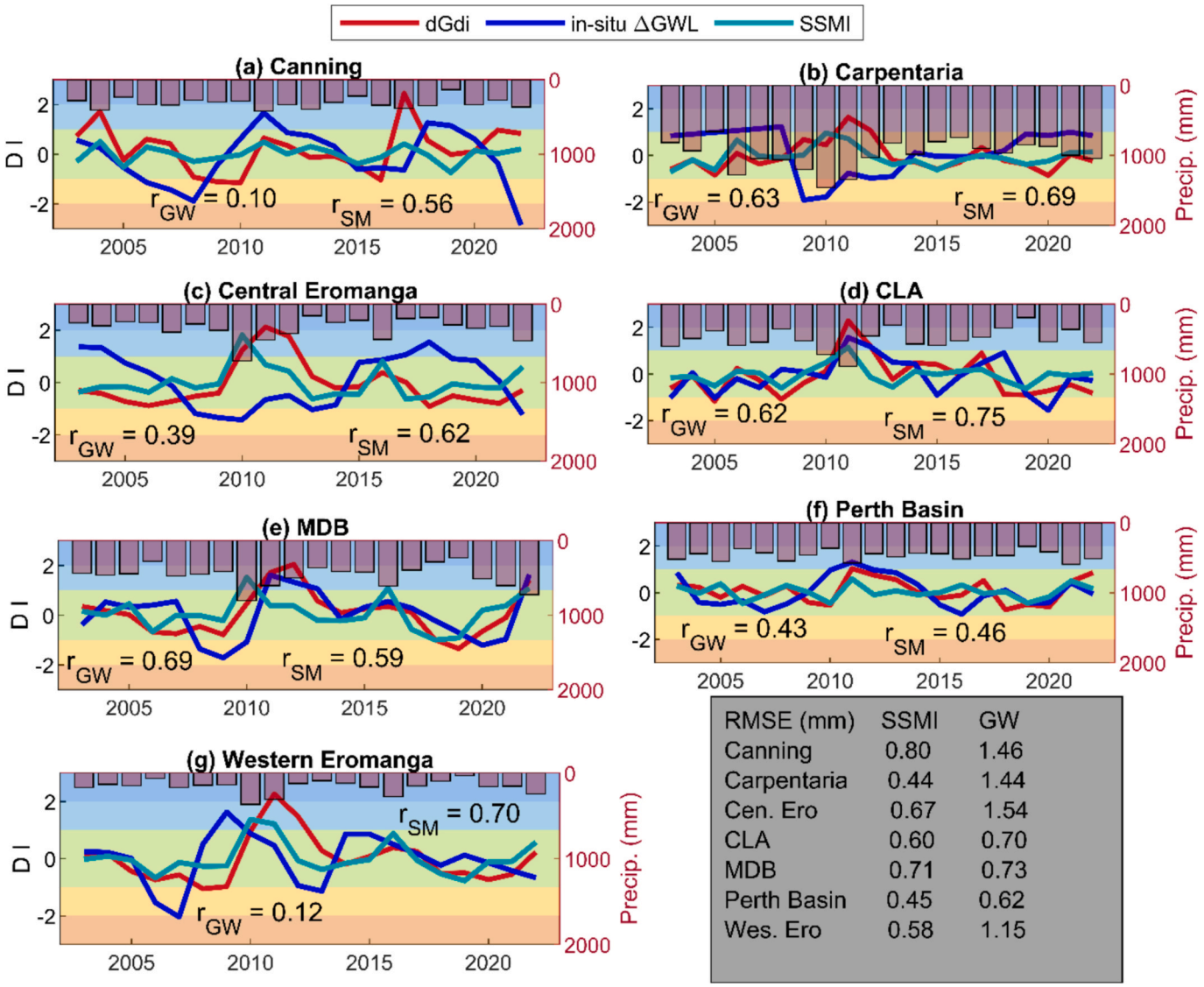

Fig. 4. Plot showing co-occurrence between annual precipitation and yearly drought events over major river basins in Australia. The light red to light blue background colours in each subplot coincides with the drought classification given in Table 2, depicting a colour progression from very dry, dry, normal, wet, and very wet conditions. The averaged annual precipitation is shown in dark red bars. The r_{GW} and r_{SM} values represent the correlation between dGdi and in-situ groundwater indices and SSMI, respectively. The root mean square table for the dGdi against standardized soil moisture index and in-situ groundwater levels is also shown. D. I stands for Drought indices. (For interpretation of the references to colour in this figure legend, the reader is referred to the web version of this article.)

Basins respond well to influences of rainfall translating to a predictable drought index for them.

5.2. *Validation of downscaled GRACE drought index using SPEI and NDVI*

To better understand climate influences on drought patterns across our study region, we partitioned the period into 2003 to 2009 and 2010 to 2022, with each respective period representing the Millenium drought and the post-Millenium drought era. During the Millenium and post-Milllenium drought era, the strongest monthly relationship between the dGdi and NDVI was observed in the Central and Western Eromanga basins (Fig. 5c, 5 g). This strong relationship could be attributed to the region's groundwater-dependent ecosystems and arid to semi-arid climate. Vegetation in these areas relies heavily on groundwater due to limited and highly variable rainfall, making its health, as reflected in NDVI, sensitive to changes in total water storage. And since the GRACE data captures groundwater, soil moisture, and surface water anomalies, it provides a more comprehensive indicator of hydrological drought than precipitation alone. Also, groundwater is relatively shallow in these basins, allowing plants to access stored subsurface water during dry periods (Toupin et al., 1997; Department of Climate Change, 2024).

For the SPEI values, the Carpentaria, Central Eromanga, MDB, and Western Eromanga all showed strong relationships during the Millenium drought era; however, after the rains, they all recorded low relationships except the MDB (Fig. 5e). This is mostly because, unlike the other basins, the MDB experienced two clear episodes of water storage recharge and decline during our study period (Fig. 4e), increasing its sensitivity to precipitation and evaporation. This led to a higher relationship with the SPEI during and after the Millenium drought.

Following the heavy rains in 2009/2010 that ended the Millenium drought, we observe that the dGdi of all the basin were propelled into wet and very wet periods during the same period, except the Canning and Perth Basins. This is because these basins are located in western Australia, where the impacts of the drought were less severe, and significant rainfall events between 2009 and 2010 were not recorded. Rather, rainfall patterns have steadily declined since the 1970 s (as

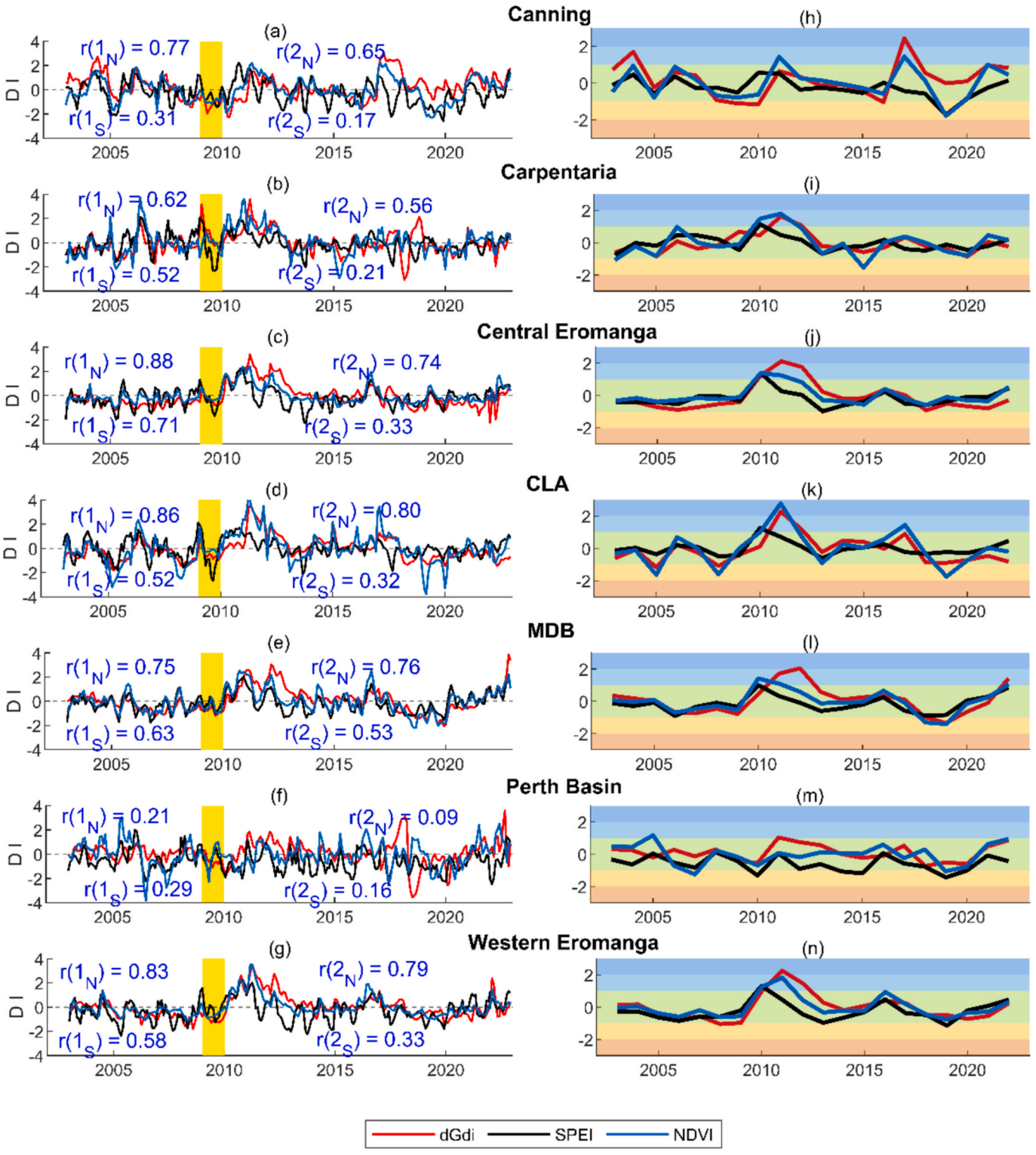

Fig. 5. Monthly (a-g) and annual (h-n) comparison of the downscaled GRACE drought index (dGdi) with well-known indices of SPEI and NDVI. The yellow vertical line in (a-g) highlights the heavy rainfall that was witnessed within southeast Australia, which ended the Millenium drought era. In panels (a-g), $r(1_N)$ and $r(2_N)$ represent the correlation between dGdi and NDVI for the Millenium drought and post Millenium drought eras, respectively, while $r(1_S)$ and $r(2_S)$ represent the correlation between dGdi and SPEI for the Millenium drought and post Millenium drought eras, respectively. The light red to light blue background colours in subplots h-n coincide with the drought classification given in Table 2 and depict a colour progression from very dry, dry, normal, wet, and very wet conditions. The left y-axis relates to the dGdi, SPEI, and NDVI values. D. I stands for Drought indices. (For interpretation of the references to colour in this figure legend, the reader is referred to the web version of this article.)

opposed to short-term drought-flood events) (Smith & Power, 2014).

Fig. 5h–5n shows the annual time series of the dGdi against the SPEI and NDVI indices. The annual correlation (r) between our downscaled GRACE index and these indices across all basins, Canning (*SPEI = 0.12, NDVI = 0.73*), Carpentaria (*SPEI = 0.41, NDVI = 0.80*), Central Eromanga (*SPEI = 0.50, NDVI = 0.85*), CLA (*SPEI = 0.48, NDVI = 0.88*), MDB (*SPEI = 0.57, NDVI = 0.82*), Perth Basin (*SPEI = 0.47, NDVI = 0.35*), Western Eromanga (*SPEI = 0.50, NDVI = 0.86*) reveal that our approach conforms with other well-known drought indices and is reliable for use, regardless of the season. The downscaled GRACE drought indices in the MDB maintained the strongest correlation for SPEI values, while the CLA maintained the strongest correlation for the NDVI values. This could be because both Basins are strongly involved in interactions between surface and groundwater systems, strongly supported by consistent rainfall patterns every year (Fig. 4). Also, the CLA has had very limited land clearing (compared to the other regions) and the vegetation is highly responsive to fluctuations in the rainfall patterns.

5.3. Spatio-temporal variability of drought evolutions

We analysed the spatio-temporal evolutions of drought conditions across the study region using the downscaled GRACE drought indicator proposed in this study. This is summarised based on the seven major river basins in Australia and shown in Fig. 6. Between 2003 and 2009, the basins mostly witnessed very dry conditions, reflecting the ongoing drought period. However, the signal is more complicated in northern Australia, where the Millennium Drought had limited influence. The Carpentaria basin, which is usually very wet, maintained a consistent dry regime for three years (2003 to 2005) but otherwise showed normal to wet conditions. The MDB and Eromanga basins were largely dry to very dry from 2006 to 2009, while, between 2010 and 2012, when heavy rains came (coinciding with a strong La Nina event), we observed very wet conditions for all the river basins, except the Canning and Perth Basins (the latter is not clearly shown in Fig. 6 due to spatial size).

After the heavy rains that impacted on most basins from 2010 to 2012, most river basins adjusted to their normal hydrological conditions, and this action peaked in 2018 when all the basins experienced drier-than-normal conditions. One notable basin that exhibited exceptional hydrological signals was the Canning Basin. From 2008 to 2016, this basin consistently showed very dry conditions (with some short periods of wet conditions in individual years). This was not due to the absence of rainfall during these periods, as we observe that rainfall within this period was normal (albeit very minimal), with exceptions to 2015 and 2019, where very low annual rainfall was reported (Fig. 4). Limited in-situ groundwater data in this region necessitated strong interpolation (Table 1) to analyze groundwater level behaviour, limiting the reliability of the in-situ groundwater analysis. However, we can report that this basin is a hotspot for mining (Department of Water,

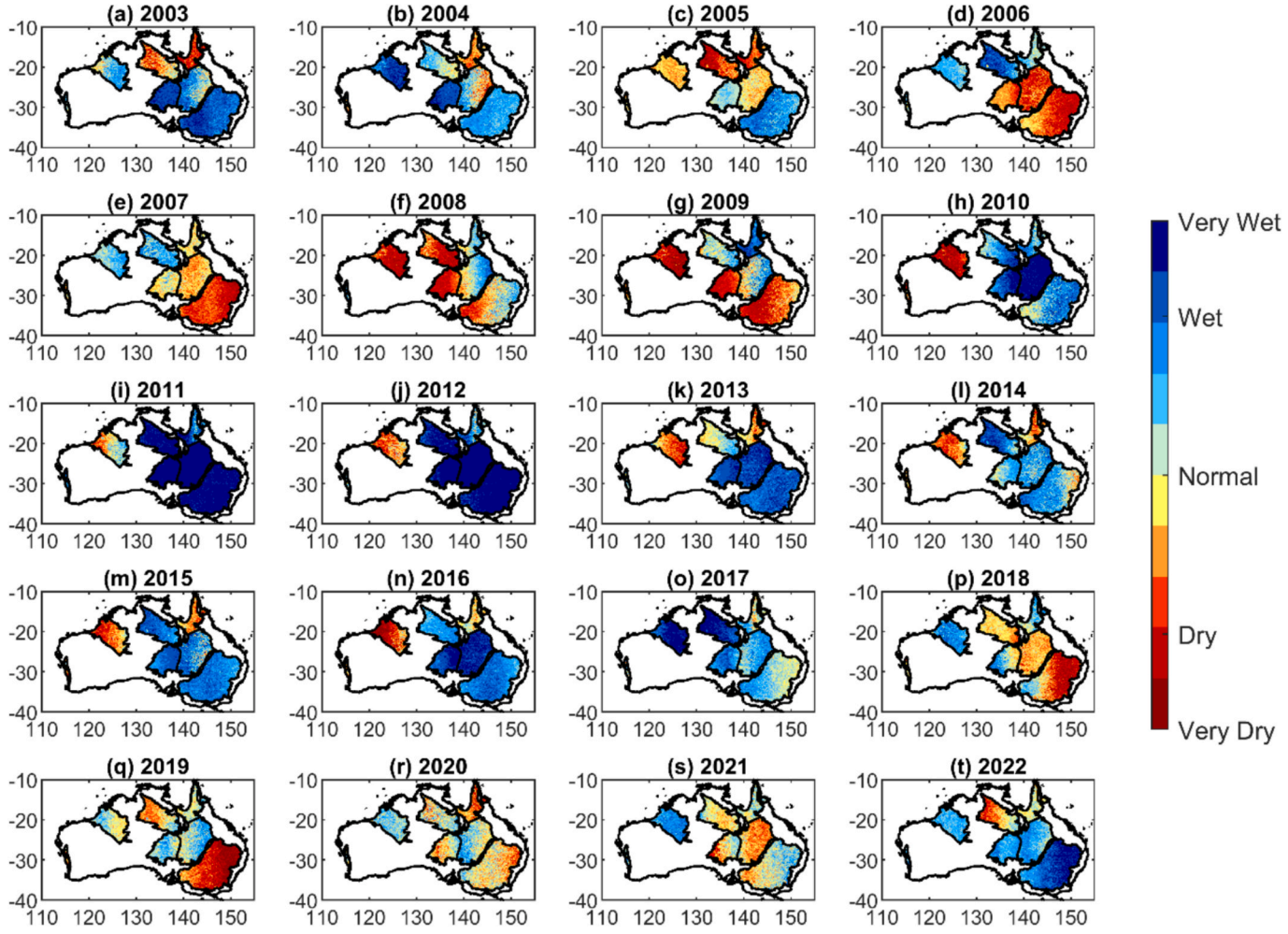

Fig. 6. Spatio-temporal pattern of the dGdi for seven major basins in Australia, including the Canning, Carpentaria, Central Eromanga, CLA, MDB, Perth and Western Eromanga Basins for the study period. The classification of the dGdi values is based on Table 2 where dark red and dark blue represents severely dry and wet periods, respectively. The yellow colour represents normal conditions. *Monthly dGdi dataset is averaged for each year (2003 to 2022).* (For interpretation of the references to colour in this figure legend, the reader is referred to the web version of this article.)

2012). If the region's groundwater resources are being used to support mining and other industry, it is plausible that this basin will suffer from long-term drought conditions induced by high water extraction rates. This condition is also observed in the original GRACE drought signals (Fig. S2).

5.4. Seasonal and long-term drought

The duration of seasonal droughts varied significantly across the study basins, reflecting their heterogeneous hydrological characteristics. For example, in Fig. 7, we observe that drought intensifies between October and November for the Canning (Fig. 7a), the Carpentaria (Fig. 7b), the Central Eromanga (Fig. 7c), the CLA (Fig. 7d), the MDB (Fig. 7e), the Western Eromanga (Fig. 7g) basins, and they experience wet conditions around March. This is in line with their seasonal dry and wet cycles (Leblanc et al., 2012; Wang et al., 2021). This means that during periods of drought, the dry season reaches drier-than-average conditions, while the wet season might still show wet episodes. Conversely, the Perth basin exhibits inconsistent seasonal patterns due to its unique hydrological patterns, land use, seasonal cycle and teleconnection influences, which aligns with previous findings (Kalu et al., 2024c).

The correlation between the variables in Fig. 7 is also observed. The MDB maintained the strongest seasonal relationship between the dGdi and the SPEI at $r = 0.75$, the CLA maintained the strongest relationship between dGdi and in-situ GWL at $r = 0.99$. In contrast, the Carpentaria and Central Eromanga Basin maintained the strongest relationship between dGdi and NDVi at $r = 0.95$, respectively. While the MDB, CLA, and Carpentaria regions are very significant basins in Australia where surface water-driven systems interact with major rivers and tributaries, Perth Basin's water resources are dominated by groundwater – and has been reported to have had limited inflow to surface water storages since the early 2000 s (Water Corporation, 2025 Jan 5). These basins are highly developed as they are known to experience steady seasonal precipitation patterns.

While the Perth Basin exhibited a weak seasonal relationship due to its hydrological conditions, the Central Eromanga, on the other hand, maintained an average seasonal relationship between dGdi and SPEI, in-situ GWL, and NDVI. This could be because this region is very dry and witnesses some groundwater extraction from its confined sandstone aquifers (it comprises a major portion of the Great Artesian Basin) (Moss & Wake-Dyster, 1983). These operations might impact the land surface conditions and limit our understanding of seasonal drought evolutions.

Because long-term drought can significantly impact hydrological systems, ecosystems, and human operations (Table S1), it is important to understand the evolution of long-term drought in our study regions. Even though many studies limit long-term drought assessments to 36 months, we explore decadal long-term drought evolutions for up to 216 months (Fig. 8). For the first 12 months, we observe that the Carpentaria Basin and CLA show dry signals, whereas the other Basins show wet signals. This dry phenomenon perseveres for 72 months and extends to the Central Eromanga Basin. It is important to note that drought characteristics in each region differ based on their unique hydrological properties, and this means that a relatively wetter region like the Carpentaria getting less land water can be characterised as drought. In contrast, that same exact condition might not mean drought in other basins. In the next 108 months, all the river basins are clear of all dry signals, and all show wet signals except the Canning Basin, where the signals are extremely dry. This condition persists into the 216th month, showing that the long-term drought influence over the Canning Basin strongly impacts the hydrological systems, ecosystems, and human operation there. It also affected groundwater storage, soil moisture and surface water availability. The spatial representation of dry river basins across most of CLA, Canning and Central Eromanga in Fig. 8 was also reported in the Australian Combined Drought Indicator developed by Guillory et al. (2023).

While short-term drought evolutions witnessed in the Carpentaria and the CLA can stress crop production and reservoir levels in those regions, long-term drought evolution witnessed in the Canning Basin shows the possibility of leading to permanent shifts in the region's ecosystem composition, land degradation, and aquifer depletion. This is intensified because of the low rainfall rates in the Canning Basin. Therefore, more studies are required over the Canning Basin to inform management actions to avert any potential permanent negative

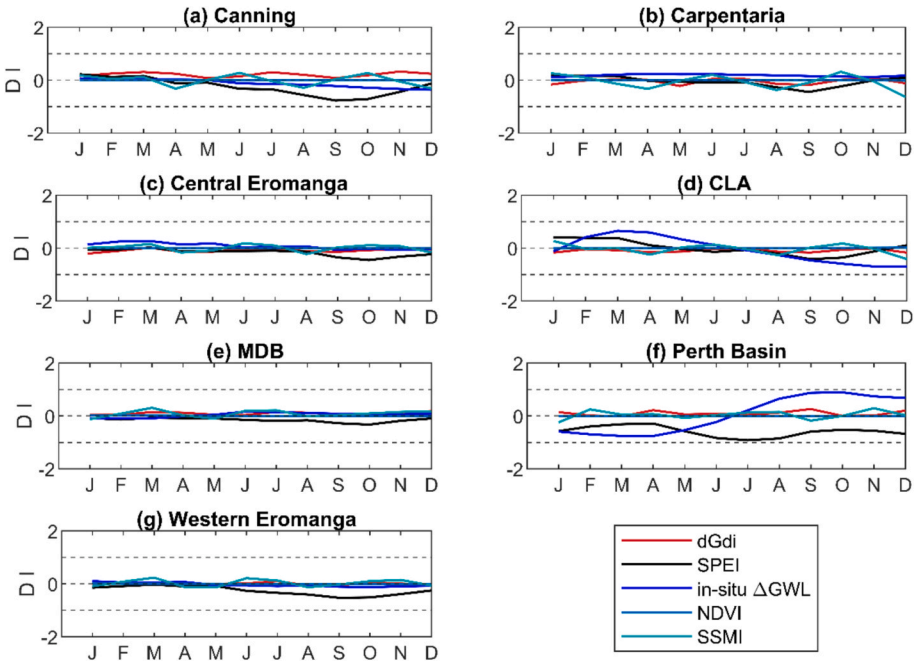

Fig. 7. Seasonal trends of hydrological drought indices for the downscaled GRACE products, SPEI, in-situ GWLs, and NDVI. The left y-axis relates to the dGdi, SPEI, and in-situ ΔGWL while the right y-axis relates to the NDVI values, whose range warranted its separation from the other indices. The dashed horizontal lines in the left y-axis correspond to the drought classification in Table 2 depicting very dry, dry, normal, wet, and very wet conditions.

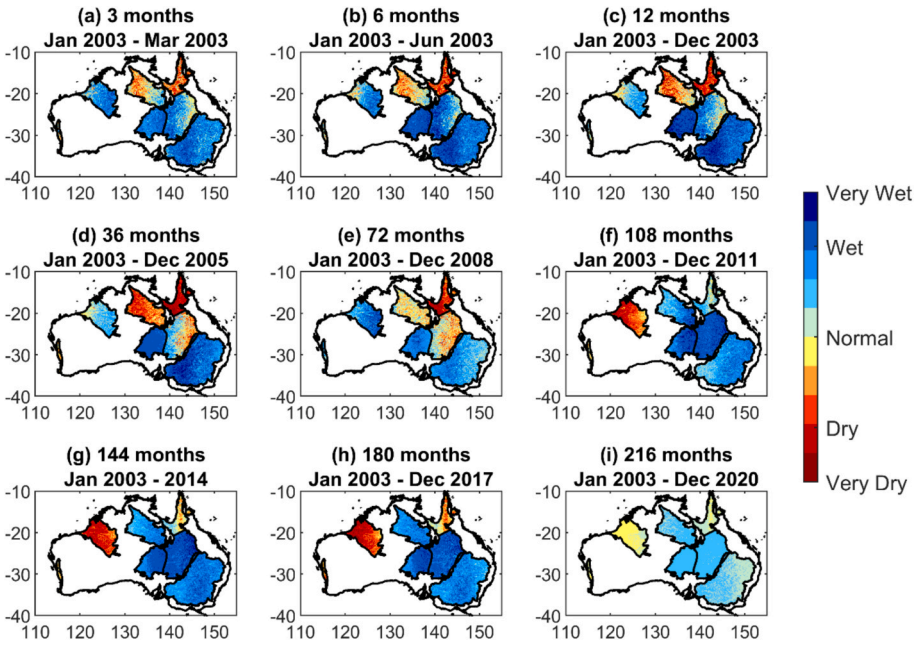

Fig. 8. Long-term (decadal) drought evolutions across major basins in Australia. The classification of the dGdi values is based on Table 2 where dark red and dark blue represents severely dry and wet periods, respectively. The yellow colour represents normal conditions. (For interpretation of the references to colour in this figure legend, the reader is referred to the web version of this article.)

hydrological and ecosystem changes in the region.

5.5. Hotspots of climatic influence

Fig. 9 presents the temporal relationship between the dGdi for all river basins and global teleconnection patterns from the Indian and Pacific Oceans. Specifically, we examined the influence of various teleconnections on the drought conditions across different basins to identify basins whose drought progressions are worsened by teleconnection impacts. While our experiment reveals low influence from the global indices in Australia's drought progression, we identified some basins that are susceptible to these climate actions. For example, the Perth Basin witnessed a correlation of 0.41 and 0.43 from ENSO and ONI, respectively. This played a key role in the inconsistent patterns exhibited in the annual signals of dGdi, SPEI, NDVI and in-situ GWLs over the Perth Basin. Also, the Perth Basin's proximity to the ocean makes it highly vulnerable to sea level pressure systems in the North Pacific High, which are known to regulate weather patterns and sometimes result in inconsistent climatology (Ndehedehe & Adeyeri, 2024).

Fig. 9 provides a comprehensive review of how different oceanic indices contribute to regional drought dynamics (Ndehedehe et al., 2020; Wang et al., 2020; Ndehedehe et al., 2021; Adeyeri et al., 2023) and serves as a foundation for the subsequent analysis of deep learning-based predictions, as illustrated in Fig. 10.

The global indices, including ENSO, NOI, ONI, PDO, QBO, and IOD, which reflect influences from the nearby Pacific and Indian oceans, were used to train the model for each respective basin. Results from the deep learning analysis showed how specific climate indices influenced drought patterns in each region. The 30 % test results showing the influence of these teleconnection patterns on our downscaled GRACE drought index is shown in Fig. 10.

Our results show that the influence of teleconnection patterns is strongest in the Canning and the Central Eromanga Basins (Fig. 10a, 10c). The indices with the strongest influences in these basins were ENSO, ONI, and IOD. This highlights signals from the Pacific and Indian Oceans and shows their contributions, however minimal, to Australian drought evolutions. We also observe that the CLA has the weakest influence of the teleconnection pattern on its drought evolution (Fig. 10d) and was mostly driven by signals from ENSO and IOD. The BPNN deep learning method in this study did not show very strong climate influences on the Perth Basin, as observed in the temporal relationship in Fig. 9. This could be due to the time-lag effect between drought occurrence and the global index or the limited training data volume/bias. Notwithstanding, other deep learning methods can be explored in future studies to underscore their usefulness in modelling the impacts of global climate on drought evolutions across the Perth Basin.

5.6. Benefits of downscaled GRACE drought assessments

The original GRACE drought index provides useful information regarding the terrestrial water storage changes that influence drought evolution and recovery (Liu et al., 2020) and has been shown to be consistent with other well-known drought indicators, including the US Drought Monitor (Houborg et al., 2012). Our approach of downscaling the GRACE product entails integrating it with key water budget terms, which are the hydrological fluxes responsible for these drought events. Therefore, our downscaled GRACE drought index has the potential and capability of detecting drought evolutions that may not be captured based on total water storage anomalies alone. Overall, the dGdi produced in this study agrees reasonably well with the SPEI and NDVI, which are well-known drought indices (Fig. 5, Table 3). This is expected because, while the SPEI and NDVI estimate droughts based on different conditions, the dGdi can assimilate all these conditions to provide a hybrid assessment of drought conditions. This means that the NDVI measures drought solely by focusing on vegetation greenness and health, which is well known to respond to water availability in the root zone, linking it to subsurface hydrological conditions. On the other hand, the SPEI is based on atmospheric water deficits, focusing on precipitation and potential evapotranspiration. By so doing, it does not account for subsurface water storage, such as groundwater, which often sustains vegetation during prolonged drought regimes. This also explains why the drought index derived from the in-situ GWLs highly corresponds to the NDVI over the SPEI.

Across all the study basins, the dGdi best correlated with NDVI, especially in regions where groundwater plays significant roles in vegetation survival during water deficits, such as the CLA, MDB, and the

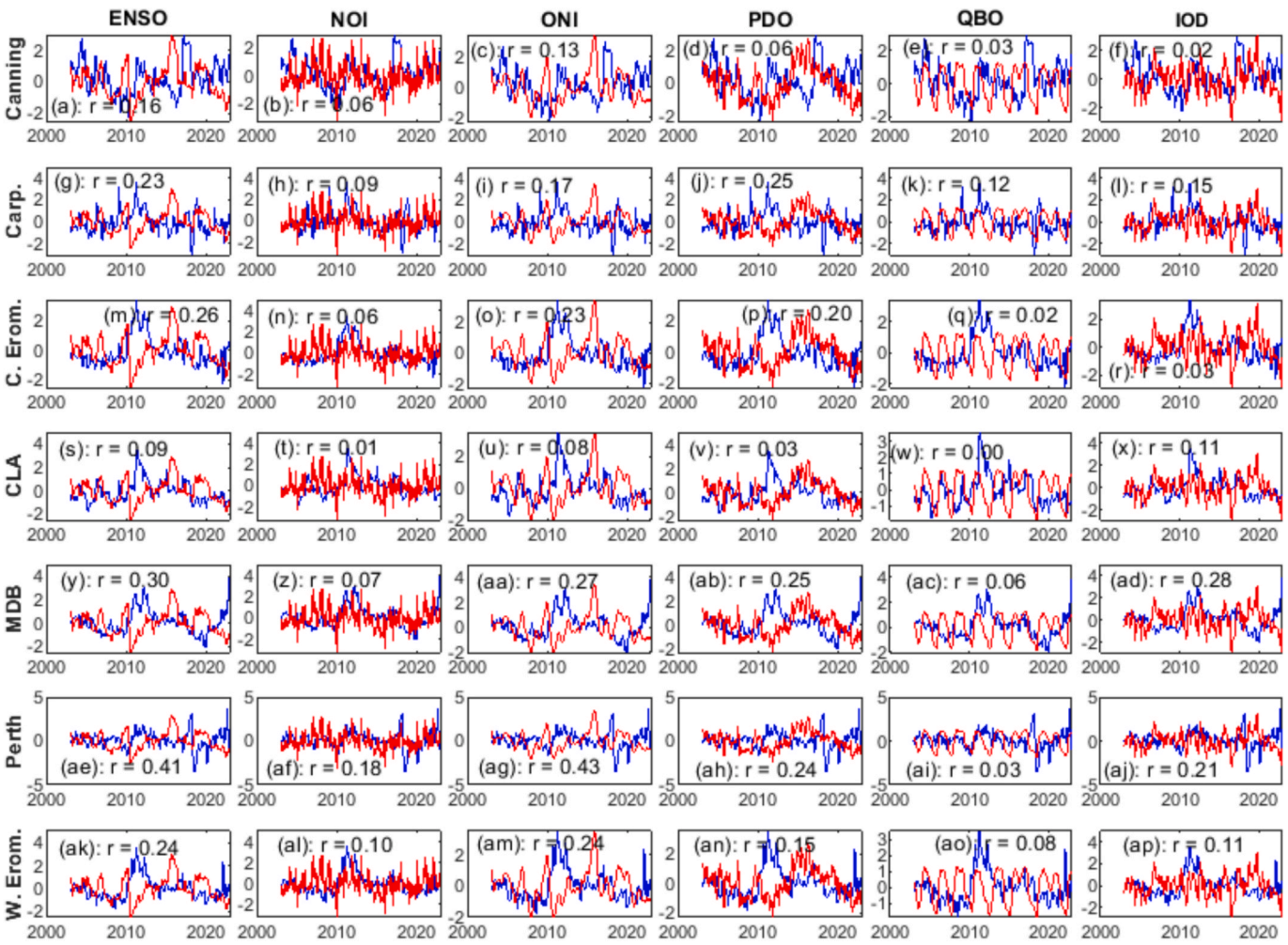

Fig. 9. Temporal relationship between the monthly downscaled GRACE drought index for all the river Basins and monthly global teleconnection patterns from the Indian and Pacific oceans. r represents the correlation coefficients between the monthly dGdi and the global teleconnection patterns explored in this study.

Eromanga Basins (Table 3). However, Fig. 9 further demonstrates the relationship between the dGdi and the global teleconnection patterns from the Indian and Pacific Oceans. This is particularly relevant in understanding how climate indices from these oceans impact drought evolution in the Australian context. Our analysis reveals that these teleconnections are not uniformly strong across all basins, with certain basins (especially those closer to the oceans, like the Perth Basin) showing a stronger correlation with indices such as ENSO, ONI, and IOD, while others exhibit weaker correlations (Fig. 9). This distinction is important for understanding regional variability in drought responses, as teleconnections like ENSO and IOD can significantly influence drought patterns by modulating atmospheric and oceanic conditions that affect water availability.

5.7. Contributions of global climate indices to Australia's drought

The downscaled GRACE drought index showed moderate links to climate teleconnection patterns, which is not surprising, as Australia's weather and climate dynamics have been shown to be influenced by these patterns (Ndehedehe et al., 2023; Wang et al., 2020). Indices from the Pacific and Indian Ocean showed moderately strong contribution to the drought events across the Perth Basin, MDB, and Western Eromanga Basins (Fig. 10). For the Carpentaria Basin, whose influences were mostly from the Indian Ocean, most of their impacts are felt around the Sheldon Lagoon, and the Skardon River areas which are known to receive the highest amount of rainfall across the entire Great Artesian Basin (Fig. S3). Basins very close to the Indian and Pacific Oceans are more susceptible to teleconnection impacts on their land water storage dynamics. This interaction depicts the importance of oceanic influences on drought patterns, particularly in regions geographically close to the bodies of water.

Another part of the Great Artesian Basin strongly influenced by these indices is the Central and Western Eromanga Basin. Both Basins are relatively arid compared to other productive basins but are impacted by the influence of ENSO, ONI, and IOD. The Central Eromanga is mostly influenced from the east, while the Western Eromanga is mostly influenced from the West. These complex interactions between teleconnection patterns suggest that their combined effects not only affect the drought evolutions in these basins, but can potentially affect the basin's groundwater recharge, surface water availability, and ecological dynamics across these regions.

The MDB and Perth Basin have been shown to be hotspots for these teleconnection patterns. Both Basins are influenced by ENSO, ONI, PDO, and IOD, especially due to their proximity to the Pacific and Indian Oceans, respectively. The influence of these patterns on the MDB is strongest in the western part of the basin and spreads to the other parts from there, whereas the central part of the Perth Basin receives the strongest influence of these patterns. The Central part of the Perth Basin is mostly urban, and it houses the Gnangara groundwater system, which contains local groundwater flow systems such as the Gingin (portion south of the Moore River) and the Perth (portion north of the Swan River). These surface and groundwater resources are very active sources

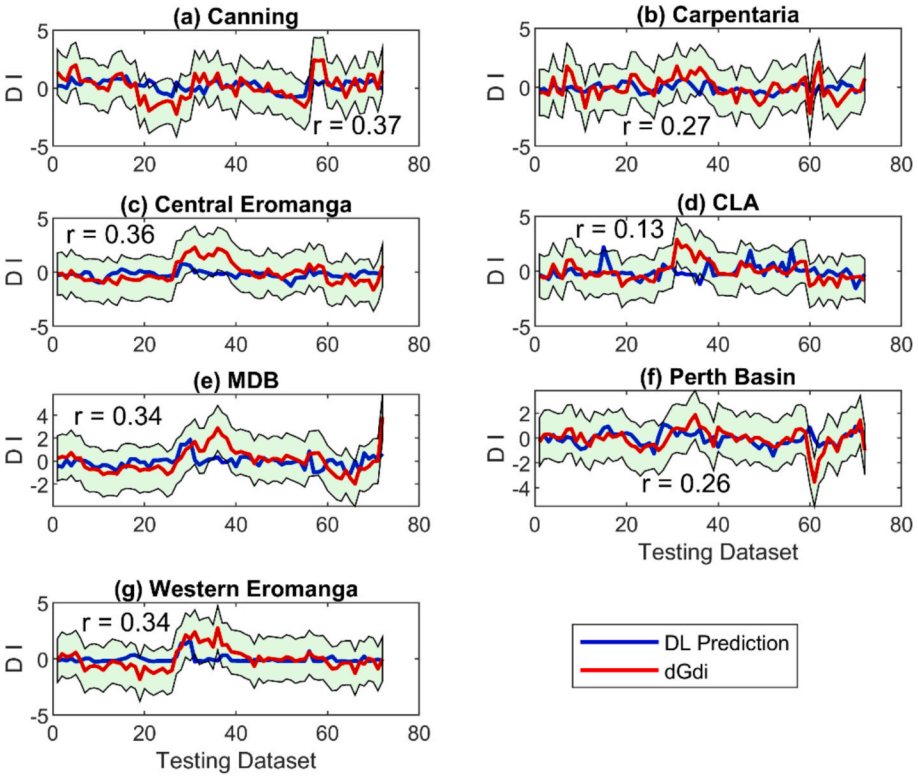

Fig. 10. Assessing the contribution of global climate indices on Australia's drought system using deep learning. The red lines represent the deep-learning drought prediction for each respective basin, while the blue lines represent the 30% testing dataset for dGdi. The green shades represent 90% confidence intervals for dGdi. (For interpretation of the references to colour in this figure legend, the reader is referred to the web version of this article.)

Table 3
Relationship of monthly downscaled GRACE drought index values with SPEI, in-situ GWL index, NDVI, and SSMI from 2003 to 2022. The values in this table are derived from Spearman's correlation coefficient. These correlation values are statistically significant.

Basin	SPEI	In-situ GWL index	NDVI	SSMI
Canning	0.20	0.10	0.47	0.20
Carpentaria	0.32	0.41	0.22	0.39
Central Eromanga	0.43	0.35	0.67	0.44
CLA	0.33	0.47	0.51	0.31
MDB	0.52	0.65	0.51	0.50
Perth Basin	0.17	0.16	0.10	0.11
Western Eromanga	0.40	0.10	0.75	0.49

of freshwater for the inhabitants of Western Australia. Because these regions directly interface with the Indian Ocean, the location is a geographic and hydrological hotspot for ocean influences on climate and drought evolutions, as captured in Figs. 9 and 10.

5.8. *Uncertainties and future direction*

Assessing the uncertainties associated with the downscaled drought index provided in this study can be challenging, especially due to the limited options available to validate downscaled GRACE datasets. However, we use in-situ monitoring bores for this operation because (i) they provide a reliable estimate of water storage dynamics in most regions where groundwater drives ΔTWS, and (ii) they are mostly localized, reflecting on water storage conditions on very local scales. For our study, we could not get 'quality A' (quality A refers to the best quality of groundwater observations) monitoring bores across all the sub-basins studies, especially over the Canning, Carpentaria, Central Eromanga, and Western Eromanga Basins. This is because these Basins have limited bores available to the public. We used linear interpolation to fill most of the data gaps from these bores, which might influence their integrity to serve as validation tools for the downscaled GRACE datasets.

In addition, we directly used GWL for our index assessments without converting them to storages. This was done because, the conversion of GWLs to storages require multiplying the bore estimates with storage coefficients and specific yield of the respective aquifers. These parameters are rarely observed and are difficult to obtain for most regions due to the difficulty of estimating these storage coefficients and specific yield values, especially for large-scale aquifers with varying rock and geological formations (Kuang et al., 2020). Therefore, including them could introduce large uncertainties to the drought index computed based on the in-situ GWLs. Also, in-situ GWLs do not always capture the full spectrum of drought types – such as, meteorological, agricultural, and hydrological droughts. As such, discrepancies between dGdi and in-situ GWL indices can be expected, especially when drought conditions primarily affect surface systems or soil moisture rather than deep aquifers. Furthermore, the use of in-situ bore data for validation was driven by the limited availability of comprehensive ground-truth datasets for satellite-based observations such as GRACE. While useful, these point-based measurements do not fully represent the spatial heterogeneity of drought processes across the entire basin and should be interpreted as partial indicators rather than definitive validation tools.

Looking ahead, however, with the expected advancement of new satellite and modelling techniques for groundwater and surface water explorations, the science of direct observation of high-resolution groundwater and surface water storages will become possible. Next-generation gravimetric satellite datasets leveraging the surface water and ocean topography (SWOT) satellite and the improved soil moisture models will provide a highly accurate system for disaggregating the vertical GRACE signals (Altenau et al., 2021; Huang et al., 2023). This will support drought studies by providing unique and accurate data layers of land water stores where hydrological drought assessments can be done based on the specific climatic and hydrological conditions of the

region like Australia. Additionally, a high-resolution (or downscaled) GRACE drought index offers an opportunity to build on the recently developed GPS-GRACE multivariate drought index (Lenczuk et al., 2024). A downscaled GRACE Drought Severity Index and GPS-derived vertical displacements warrants further evaluation to enhance the detection of short-term hydrological changes at local scales. The improved accuracy of these systems will likely transform drought studies, facilitating more accurate monitoring and management of water resources.

6. Conclusion

In this study, we propose a drought index based on downscaled or high spatial resolution GRACE TWSA products and characterized drought evolutions across major river basins in Australia from 2003 to 2022. The downscaled GRACE drought indicator is an improvement on the original GRACE-based drought indicator due to the addition of key hydrological flux variables responsible for global drought occurrences, including precipitation, evapotranspiration, runoff and deep drainage. We summarize the key takeaways from this study below:

(i) The downscaled GRACE drought indicator is very useful in drought assessments because it agrees with well-known indices of SPEI, NDVI, and even drought indices from in-situ groundwater bores and standardized soil moisture indices. The strong agreement observed with these indices across different Australian landscapes shows that the product can be very useful to detect complex hydro-climatic drought progressions. The same approach could be successfully used in other regions beyond Australia in future.
(ii) Most of the recorded drought episodes across the basins were predominantly agricultural in nature, characterised by shallow soil moisture deficits rather than significant groundwater depletions.
(iii) The downscaled GRACE drought indicator revealed a long-term drought evolution for up to 216 months. It showed that the Canning Basin is facing long-term drought and reveals that the region risks permanent shifts in ecosystem composition and land degradation associated with aquifer depletion.
(iv) ENSO, ONI, and IOD climate teleconnection patterns contribute most to the drought progression in Australia, especially over river Basins that are close to the oceans.

Finally, our analysis demonstrates that the proposed downscaled GRACE drought index can be a useful tool for integrated drought monitoring across varying climates and landscapes, thus providing a reliable metric for drought preparedness and adaptation in Arid Australia.

7. Open Research

GRACE dataset: https://www2.csr.utexas.edu/grace/
PCP, ET, RO, D2, RZSM datasets: https://awo.bom.gov.au/products/
SPEI: https://digital.csic.es/handle/10261/332007.
NDVI: https://lpdaac.usgs.gov/products/mod13a1v061/
In-situ monitoring bores: http://www.bom.gov.au/water/groundwater/explorer/map.shtml

CRediT authorship contribution statement

Ikechukwu Kalu: Writing – review & editing, Writing – original draft, Visualization, Validation, Software, Methodology, Investigation, Formal analysis, Data curation, Conceptualization. **Christopher E. Ndehedehe:** Writing – review & editing, Visualization, Supervision, Software, Resources, Project administration, Investigation, Funding acquisition, Formal analysis, Conceptualization. **Vagner G. Ferreira:** Writing – review & editing, Visualization, Supervision, Methodology, Investigation, Formal analysis. **Sreekanth Janardhanan:** Writing – review & editing, Software, Resources, Project administration, Funding acquisition, Data curation. **Matthew Currell:** Writing – review & editing, Visualization, Validation, Supervision, Investigation. **Oluwafemi E. Adeyeri:** Writing – review & editing, Validation, Investigation, Formal analysis, Visualization. **Onuwa Okwuashi:** Writing – review & editing, Visualization, Validation, Software, Methodology. **Mark J. Kennard:** Supervision, Software, Resources, Project administration, Investigation, Funding acquisition, Writing – review & editing, Visualization, Validation.

Declaration of competing interest

The authors declare that they have no known competing financial interests or personal relationships that could have appeared to influence the work reported in this paper.

Acknowledgements

The authors are grateful to the Australian Bureau of Meteorology, the National Aeronautics and Space Administration (NASA), and the Commonwealth Scientific and Industrial Research Organization (CSIRO) for all the data used in this study. Ikechukwu Kalu received funding from Griffith University Postgraduate Research Scholarships and a top-up funding from CSIRO. Christopher Ndehedehe is supported by the Australian Research Council Discovery Early Career Researcher Award (DE230101327) for the project, *Assessing the impacts of drought and water extraction on groundwater resources in Australia.* Vagner Ferreira is supported by the Joint Research, Development and Application Demonstration of Remote Sensing Monitoring Technology for Typical Natural Resources Features (Grant 2023YFE0207900) and the National Natural Science Foundation of China (Grant W2432026). Oluwafemi E. Adeyeri is supported by the Australian Research Council grant number CE230100012.

Appendix A. Supplementary data

Supplementary data to this article can be found online at https://doi.org/10.1016/j.jhydrol.2025.134035.

Data availability

I have shared the link to my data in the Open Research section

References

Adeyeri, O.E., Zhou, W., Laux, P., Wang, X., Dieng, D., Widana, L.A., Usman, M., 2023. Land use and land cover dynamics: Implications for thermal stress and energy demands. Renew. Sustain. Energy Rev. 179, 113274.
Adeyeri, O.E., Zhou, W., Ndehedehe, C.E., Wang, X., Ishola, K.A., Laux, P., 2024. Minimizing uncertainties in climate projections and water budget reveals the vulnerability of freshwater to climate change. One Earth 7 (1), 72–87.
Agarwal, V., Akyilmaz, O., Shum, C.K., Feng, W., Yang, T.Y., Forootan, E., Uz, M., 2023. Machine learning based downscaling of GRACE-estimated groundwater in Central Valley, California. Sci. Total Environ. 865, 161138.
Altenau, E.H., Pavelsky, T.M., Durand, M.T., Yang, X., Frasson, R.P.D.M., Bendezu, L., 2021. The Surface Water and Ocean Topography (SWOT) Mission River Database (SWORD): a global river network for satellite data products. Water Resour. Res. 57 (7), e2021WR030054.
Askarimarnani, S.S., Kiem, A.S., Twomey, C.R., 2021. Comparing the performance of drought indicators in Australia from 1900 to 2018. Int. J. Climatol. 41, E912–E934.
BOM (2015), Australian Groundwater Explorer. Australian Groundwater Explorer Infosheet (bom.gov.au).
Burgess, W.G., Shamsudduha, M., Taylor, R.G., Zahid, A., Ahmed, K.M., Mukherjee, A., Bense, V.F., 2017. Terrestrial water load and groundwater fluctuation in the Bengal Basin. Sci. Rep. 7 (1), 3872.
Cammalleri, C., Barbosa, P., Vogt, J.V., 2019. Analysing the relationship between multiple-timescale SPI and GRACE terrestrial water storage in the framework of drought monitoring. Water 11 (8), 1672.

Chen, T., De Jeu, R.A.M., Liu, Y.Y., Van der Werf, G.R., Dolman, A.J., 2014. Using satellite based soil moisture to quantify the water driven variability in NDVI: a case study over mainland Australia. Remote Sens. Environ. 140, 330–338.

Department of Climate Change (2024). Great Artesian Basin: Basin-wide Condition Report 2024. Final Report. https://www.dcceew.gov.au/sites/default/files/documents/gab-basin-wide-condition-report.pdf.

Department of Water (2012). West Canning Basin groundwater allocation limit report, *Background information and method used to set an allocation limit for aquifers in the West Canning Basin*. Report No. 52. https://www.wa.gov.au/system/files/2022-10/West-Canning-Basin-groundwater-allocation-limit-report.pdf.

Devanand, A., Evans, J.P., Abramowitz, G., Hobeichi, S., Pitman, A.J., 2023. What is the probability that a drought will break in Australia? Weather Clim. Extremes 41, 100598.

Ferreira, V., Yong, B., Montecino, H., Ndehedehe, C.E., Seitz, K., Kutterer, H., Yang, K., 2023. Estimating GRACE terrestrial water storage anomaly using an improved point mass solution. Sci. Data 10 (1), 234.

Frost, A. J., and Shokri, A., (2021). The Australian Landscape Water Balance model (AWRA-L v7). Technical Description of the Australian Water Resources Assessment Landscape model version 7. https://awo.bom.gov.au/assets/notes/publications/AWRA-Lv7_Model_Description_Report.pdf.

Gash, J.H.C., 1979. An analytical model of rainfall interception by forests. Q. J. R. Meteorolog. Soc. 105 (443), 43–55.

Goethals, P.L., Dedecker, A.P., Gabriels, W., Lek, S., De Pauw, N., 2007. Applications of artificial neural networks predicting macroinvertebrates in freshwaters. Aquat. Ecol. 41, 491–508.

Guillory, L., Pudmenzky, C., Nguyen-Huy, T., Cobon, D., Stone, R., 2023. A drought monitor for Australia. Environ. Model. Software 170, 105852.

Halder, B., Tiyasha, T., Shahid, S., Yaseen, Z.M., 2022. Delineation of urban expansion and drought-prone areas using vegetation conditions and other geospatial indices. Theor. Appl. Climatol. 149 (3), 1277–1295.

Houborg, R., Rodell, M., Li, B., Reichle, R., Zaitchik, B.F., 2012. Drought indicators based on model-assimilated Gravity Recovery and climate Experiment (GRACE) terrestrial water storage observations. Water Resour. Res. 48 (7).

Huang, Z., Yeh, P.J.F., Jiao, J.J., Luo, X., Pan, Y., Long, Y., Zheng, L., 2023. A new approach for assessing groundwater recharge by combining GRACE and baseflow with case studies in karst areas of southwest China. Water Resour. Res. 59 (2), e2022WR032091.

Johnston, R.M., Barry, S.J., Bleys, E., Bui, E.N., Moran, C.J., Simon, D.A.P., Grundy, M., 2003. ASRIS: the database. Soil Res. 41 (6), 1021–1036.

Jones, D.A., Wang, W., Fawcett, R., 2009. High-quality spatial climate data-sets for Australia. Aust. Meteorol. Oceanogr. J. 58 (4), 233.

Kalu, I., Ndehedehe, C.E., Okwuashi, O., Eyoh, A.E., Ferreira, V.G., 2022. An assimilated deep learning approach to identify the influence of global climate on hydrological fluxes. J. Hydrol. 614, 128498.

Kalu, I., Ndehedehe, C.E., Ferreira, V.G., Kennard, M.J., 2024a. Machine learning assessment of hydrological model performance under localized water storage changes through downscaling. J. Hydrol. 628, 130597.

Kalu, I., Ndehedehe, C.E., Ferreira, V.G., Janardhanan, S., Currell, M., Kennard, M.J., 2024b. Statistical downscaling of GRACE terrestrial water storage changes based on the Australian Water Outlook model. Sci. Rep. 14 (1), 10113.

Kalu, I., Ndehedehe, C.E., Ferreira, V.G., Janardhanan, S., Currell, M., Crosbie, R.S., Kennard, M.J., 2024c. Remote sensing estimation of shallow and deep aquifer response to precipitation-based recharge through downscaling. Water Resour. Res. 60 (12), e2024WR037360.

Kiem, A.S., Johnson, F., Westra, S., van Dijk, A., Evans, J.P., O'Donnell, A., Mehrotra, R., 2016. Natural hazards in Australia: droughts. Clim. Change 139, 37–54.

Krishnamurthy, L., Krishnamurthy, V., 2016. Decadal and interannual variability of the Indian Ocean SST. Clim. Dyn. 46, 57–70.

Kuang, X., Jiao, J.J., Zheng, C., Cherry, J.A., Li, H., 2020. A review of specific storage in aquifers. J. Hydrol. 581, 124383.

Leblanc, M.J., Tregoning, P., Ramillien, G., Tweed, S.O., Fakes, A., 2009. Basin-scale, integrated observations of the early 21st century multiyear drought in southeast Australia. Water Resour. Res. 45 (4).

Leblanc, M., Tweed, S., Van Dijk, A., Timbal, B., 2012. A review of historic and future hydrological changes in the Murray-Darling Basin. Global Planet. Change 80, 226–246.

Lenczuk, A., Ndehedehe, C., Klos, A., Bogusz, J., 2024. A new Multivariate Drought Severity Index to identify short-term hydrological signals: case study of the Amazon River basin. Remote Sens. Environ. 315, 114464.

Liu, X., Feng, X., Ciais, P., Fu, B., Hu, B., Sun, Z., 2020. GRACE satellite-based drought index indicating increased impact of drought over major basins in China during 2002–2017. Agric. For. Meteorol. 291, 108057.

McKee, T.B., Doesken, N.J., Kleist, J., 1993. The relationship of drought frequency and duration to time scales. In: Proceedings of the 8th Conference on Applied Climatology, pp. 179–183.

Miro, M.E., Famiglietti, J.S., 2018. Downscaling GRACE remote sensing datasets to high-resolution groundwater storage change maps of California's Central Valley. Remote Sens. (Basel) 10 (1), 143.

Moss, F.J., Wake-Dyster, K.D., 1983. The Australian central Eromanga Basin project: an introduction. Tectonophysics 100 (1–3), 131–145.

Ndehedehe, C.E., Adeyeri, O.E., 2024. Changes in drought characteristics and heatwave propagation over groundwater basins in Australia. Earth Syst. Environ. 1–20.

Ndehedehe, C.E., Adeyeri, O.E., Onojeghuo, A.O., Ferreira, V.G., Kalu, I., Okwuashi, O., 2023. Understanding global groundwater-climate interactions. Sci. Total Environ. 904, 166571.

Ndehedehe, C.E., Agutu, N.O., Ferreira, V.G., Getirana, A., 2020. Evolutionary drought patterns over the Sahel and their teleconnections with low frequency climate oscillations. Atmos. Res. 233, 104700.

Ndehedehe, C.E., Awange, J.L., Kuhn, M., Agutu, N.O., Fukuda, Y., 2017. Climate teleconnections influence on West Africa's terrestrial water storage. Hydrol. Process. 31 (18), 3206–3224.

Ndehedehe, C.E., Ferreira, V.G., Agutu, N.O., Onojeghuo, A.O., Okwuashi, O., Kassahun, H.T., Dewan, A., 2021. What if the rains do not come? J. Hydrol. 595, 126040.

Ning, S., Ishidaira, H., Wang, J., 2014. Statistical downscaling of GRACE-derived terrestrial water storage using satellite and GLDAS products. 土木学会論文集 B1 (水工学) 70 (4), I_133-I_138.

Patil, P.P., Jagtap, M.P., Khatri, N., Madan, H., Vadduri, A.A., Patodia, T., 2024. Exploration and advancement of NDDI leveraging NDVI and NDWI in Indian semi-arid regions: a remote sensing-based study. Case Stud. Chem. Environ. Eng. 9, 100573.

Peel, M.C., Finlayson, B.L., McMahon, T.A., 2007. Updated world map of the Köppen-Geiger climate classification. Hydrol. Earth Syst. Sci. 11 (5), 1633–1644.

Phillips, T., Nerem, R.S., Fox-Kemper, B., Famiglietti, J.S., Rajagopalan, B., 2012. The influence of ENSO on global terrestrial water storage using GRACE. Geophys. Res. Lett. 39 (16).

Pillai, P.A., Mohankumar, K., 2010. Individual and combined influence of El Nino–Southern oscillation and Indian Ocean dipole on the tropospheric biennial oscillation. Quart. J. Royal Meteorol. Soc. J. Atmosph. Sci. Appl. Meteorol. Phys. Oceanogr. 136 (647), 297–304.

Save, H., Bettadpur, S., Tapley, B.D., 2016. High-resolution CSR GRACE RL05 mascons. J. Geophys. Res. Solid Earth 121 (10), 7547–7569.

Schwing, F.B., Murphree, T., Green, P.M., 2002. The Northern Oscillation Index (NOI): a new climate index for the northeast Pacific. Prog. Oceanogr. 53 (2–4), 115–139.

Shi, L., Feng, P., Wang, B., Li Liu, D., Yu, Q., 2020. Quantifying future drought change and associated uncertainty in southeastern Australia with multiple potential evapotranspiration models. J. Hydrol. 590, 125394.

Smith, I., Power, S., 2014. Past and future changes to inflows into Perth (Western Australia) dams. J. Hydrol.: Reg. Stud. 2, 84–96.

Spinoni, J., Barbosa, P., De Jager, A., McCormick, N., Naumann, G., Vogt, J.V., Mazzeschi, M., 2019. A new global database of meteorological drought events from 1951 to 2016. J. Hydrol.: Reg. Stud. 22, 100593.

Thomas, B.F., Famiglietti, J.S., Landerer, F.W., Wiese, D.N., Molotch, N.P., Argus, D.F., 2017. GRACE groundwater drought index: Evaluation of California Central Valley groundwater drought. Remote Sens. Environ. 198, 384–392.

Thomas, A.C., Reager, J.T., Famiglietti, J.S., Rodell, M., 2014. A GRACE-based water storage deficit approach for hydrological drought characterization. Geophys. Res. Lett. 41 (5), 1537–1545.

Toupin, D., Eadington, P.J., Person, M., Morin, P., Wieck, J., Warner, D., 1997. Petroleum hydrogeology of the Cooper and Eromanga basins, Australia: some insights from mathematical modeling and fluid inclusion data. AAPG Bull. 81 (4), 577–603.

Van Dijk, A., 2010. The Australian Water Resources Assessment System. Landscape Model (version 0.5). Technical Report 3. CSIRO, Australia.

Van Dijk, A.I.J.M., Bruijnzeel, L.A., 2001. Modelling rainfall interception by vegetation of variable density using an adapted analytical model. Part 1. Model description. J. Hydrol. 247 (3–4), 230–238.

Van Dijk, A.I., Beck, H.E., Crosbie, R.S., De Jeu, R.A., Liu, Y.Y., Podger, G.M., Viney, N. R., 2013. The Millennium Drought in southeast Australia (2001–2009): Natural and human causes and implications for water resources, ecosystems, economy, and society. Water Resour. Res. 49 (2), 1040–1057.

Van Loon, A.F., 2015. Hydrological drought explained. Wiley Interdiscip. Rev. Water 2 (4), 359–392.

Vicente-Serrano, S.M., Beguería, S., López-Moreno, J.I., 2010. A multiscalar drought index sensitive to global warming: the standardized precipitation evapotranspiration index. J. Clim. 23 (7), 1696–1718.

Vishwakarma, B.D., Zhang, J., Sneeuw, N., 2021. Downscaling GRACE total water storage change using partial least squares regression. Sci. Data 8 (1), 95.

Wang, W., Shen, Y., Wang, F., Li, W., 2021. Two severe prolonged hydrological droughts analysis over Mainland Australia using GRACE satellite data. Remote Sens. (Basel) 13 (8), 1432.

Wang, F., Wang, Z., Yang, H., Di, D., Zhao, Y., Liang, Q., 2020. Utilizing GRACE-based groundwater drought index for drought characterization and teleconnection factors analysis in the North China Plain. J. Hydrol. 585, 124849.

Water Corporation (2025, Jan 7). Streamflow. https://www.watercorporation.com.au/Our-water/Rainfall-and-dams/Streamflow.

Wilson, L., Bende-Michl, U., Sharples, W., Vogel, E., Peter, J., Srikanthan, S., Bellhouse, J., 2022. A national hydrological projections service for Australia. Clim. Serv. 28, 100331.

Yang, Y., Long, D., Guan, H., Scanlon, B.R., Simmons, C.T., Jiang, L., Xu, X., 2014. GRACE satellite observed hydrological controls on interannual and seasonal variability in surface greenness over mainland Australia. J. Geophys. Res. Biogeo. 119 (12), 2245–2260.